PCCP

Accepted Manuscript

This is an *Accepted Manuscript*, which has been through the Royal Society of Chemistry peer review process and has been accepted for publication.

Accepted Manuscripts are published online shortly after acceptance, before technical editing, formatting and proof reading. Using this free service, authors can make their results available to the community, in citable form, before we publish the edited article. We will replace this *Accepted Manuscript* with the edited and formatted *Advance Article* as soon as it is available.

You can find more information about *Accepted Manuscripts* in the **Information for Authors**.

σ-Aromatic Cyclic M_3^+ (M = Cu, Ag, Au) Clusters and their Complexation with Dimethyl imidazol-2-ylidene, Pyridine, Isoxazole, Furan, Noble Gas and Carbon Monoxide

Sudip Pan, Ranajit Saha, Subhajit Mandal and Pratim K. Chattaraj*

Department of Chemistry and Center for Theoretical Studies,

Indian Institute of Technology, Kharagpur, 721302, India

*Corresponding author: pkc@chem.iitkgp.ernet.in

Abstract

The σ-aromaticity of M_3^+ (M = Cu, Ag, Au) is analyzed and compared with that of Li_3^+ and prototype σ-aromatic system, H_3^+. Ligands (L) like dimethyl imidazol-2-ylidene, pyridine, isoxazole and furan are employed to stabilize these monocationic M_3^+ clusters. They all bind M_3^+ with favorable interaction energy. Dimethyl imidazol-2-ylidene forms the strongest bond with M_3^+ followed by pyridine, isoxazole and furan. Electrostatic contribution is considerably more than that of orbital contribution in these M-L bonds. The orbital interaction arises from both L→M σ donation and L←M back donation. M_3^+ clusters also bind noble gas atoms and carbon monoxide effectively. In general, among the studied systems Au_3^+ binds a given L most strongly followed by Cu_3^+ and Ag_3^+. The computation of nucleus-independent chemical shift (NICS) and its different extensions like NICS-rate and NICS in-plane component vs NICS out-of-plane component shows that the σ-aromaticity in L bound M_3^+ increases compared to that of bare cluster. The aromaticity in pyridine, isoxazole and furan bound Au_3^+ complexes is quite comparable with that in the recently synthesized $Zn_3(C_5(CH_3)_5)_3^+$. The energy gap between the highest occupied molecular orbital and the lowest unoccupied molecular orbital also increases in binding with L. The blue-shift and red-shift in C-O stretching frequency of $M_3(CO)_3^+$ and $M_3(OC)_3^+$, respectively, are analyzed through reverse polarization of the σ- and π-orbitals of CO as well as the relative amount of OC→M σ donation and M→CO π back donation. The electron density analysis is also performed to gain further insight into the nature of interaction.

Introduction

While elaborating the debate on bonding in C_2 and other systems among Frenking, Shaik, Hoffmann and Rzepa, Alvarez commented that "chemistry is all about connecting and disconnecting atoms to form new molecular or supramolecular objects. So understanding the ways in which atoms and molecules can be held together should play an important role in developing new chemistries".[1] It is indeed so and the concept of aromaticity has a dictating role about relative preference of the nature of connectivity between two atoms and the overall geometry of the molecule. Even before fully understanding the structural and bonding principles, the aromaticity, a concept introduced by Hofmann[2] in 1855, was used to rationalize the structure, stability and reactivity of a wide range of organic molecules.

It was first introduced to explain the unusual reactivity of benzene compared to their aliphatic analogues. During the early nineteenth century it was realized that despite being an unsaturated compound, benzene shows less reactivity and higher stability than those of normal alkenes and alkynes. Then, Kekulé[3] in 1865 proposed that benzene possesses a ring like texture having single and double bonds in alternating positions and since there persists two ways to obtain such arrangement, it was argued that benzene is an equilibrium mixture of two structures. However, this argument was not enough to explain the extra stability of benzene. Many scientists including Dewar with his Dewar's structure[4] and Robinson with his aromatic sextet theory[5] tried to explain the exceptional stability of benzene in subsequent years. After that, valence bond theory[6] was also employed which tends to explain the stability through resonance hybrid of two Kekulé's structures (80%) and three Dewar's structures (20%). However, it could not explain the fact that despite the electronic conjugation, cyclobutadiene does not show extra stability. Then, through his molecular orbital theory, Hückel[7] in 1931 proposed a generalized definition of aromaticity, (4n + 2) π-electron rule, for monocyclic planar systems which is widely applauded by the scientific community even today. The aromaticity criterion has since then become a very popular qualitative tool to account for an "extra stability" of a particular class of organic compounds. But, further advancement of ideas along with the growth of computational chemistry shows that the given term can be expanded into several dimensions. The aromaticity concept cannot be a monopoly of the organic chemists and can be used as well to explain the stability of purely inorganic compounds. In fact, the initial π-aromaticity concept now is expanded into σ-,

δ- and three-dimensional aromaticity.[8] In addition to that, the extension of this fascinating aromaticity concept to an all-metal Al_4^{2-} system was first attempted by Boldyrev, Wang and coworkers[9] and they launched the term, 'all-metal aromaticity'. It was then followed by a galaxy of metal clusters, which show either multiple aromaticity, conflicting aromaticity or only π- or σ-aromaticity.[10]

Actually, now-a-days the aromaticity concept is used so extensively that renowned scientist, Hoffmann[11] remarked that "today, an inflation of hype threatens this beautiful concept". His opinion is that aromatic molecules should not be reactive, and they should be bench-stable or bottleable. However, Boldyrev and Wang[12] strongly rejected his opinion remarking that aromaticity should not be reserved only for benzene and the related derivatives. Most of the scientists support the argument given by Boldyrev and Wang and opine to enjoy the many flavors of aromaticity in different systems.[12] Although aromaticity is a popular concept, it is not properly defined and accordingly cannot be computed theoretically or measured experimentally. There exists no linear hermitian operator corresponding to aromaticity in quantum mechanics. There are, however, several indirect criteria to appreciate this fascinating concept, viz., energetic or stability criterion, geometrical or symmetry criterion, magnetic criterion, reactivity criterion, etc. Surprisingly no aromatic system but for the prototypical benzene obeys all such criteria.

Owing to their application as luminescent materials and to design supramolecular networks, cyclic trinuclear complexes (CTC) of M^+ (M = Cu, Ag, Au) are very common in literature.[13] The first Au(I) CTC complex, [Au(I)₃(μ-1,2-piridyl)₃] was reported by Vaughan[14] in 1970 in which Au_3 has roughly a D_{3h} symmetry. It was then followed by the syntheses of [M₃(μ-L)₃] (M = Cu^+, Ag^+, Au^+; L = anionic ligands like pyrazolate, imidazolate, triazolates, pyridiniate and others), and their aggregates.[13c] The corresponding structures and properties are related to the closed-shell M(I)-M(I) (d^{10}-d^{10}) interaction and M(I)-L interaction. Very recently, Frenking and coworkers[15] performed theoretical studies to explore the nature of bonding in those [M₃(μ-L)₃] and they noticed aromaticity in core M_3^{3+} units. In 2012, Robilotto et al.[16] synthesized N-heterocyclic carbene (NHC), 1,3-bis(2,6-diisopropylphenyl)imidazol-2-ylidene stabilized Au_3^+, which is an isolobal analogue of σ-aromatic H_3^+. In a further recent paper, Shayeghi and coworkers[17] detected Ar supported Ag_3^+, Au_3^+ and their mixed clusters. Freitag et al.[18] observed

σ-aromaticity in Zn_3 and Zn_2Cu moieties in experimentally synthesized $Zn_3Cp*_3^+$ and Zn_2CuCp*_3 ($Cp* = C_5(CH_3)_5$) complexes in a very recent work.

In this article, we have studied the structure, stability, variation of σ-aromaticity and nature of bonding in NHC (dimethyl imidazol-2-ylidene), isoxazole (IOZ), pyridine (Py), furan (Fu), noble gas (Ng = Ar-Rn) and carbon monoxide (CO) bound M_3^+ (M = Cu, Ag, Au) clusters. Further, the σ-aromaticity of the studied systems is compared with that of Li_3^+, prototypical σ-aromatic system, H_3^+ and recently reported $Zn_3Cp*_3^+$.[18] Particular emphasis is given on the shifting of C-O stretching frequency upon complexation with M_3^+ compared to the free CO. On the appearance of C-O stretching frequency in IR-spectra the metal-carbonyl complexes are divided into two main groups. One of them is known as "classical" metal carbonyl complexes, which have C-O stretching frequency less than that in free CO due to the OC←M π back donation whereas there are many examples of metal carbonyls having C-O stretching frequency larger than that in free CO, termed as "non-classical" or "abnormal" carbonyls.[19] This increase in the C-O stretching frequency followed by a decrease in the C-O bond length in non-classical carbonyls has a long history of debate. The reason behind this effect is not only due to the OC→M σ donation but also the electrostatic effect and inverse polarization in CO moiety is liable for increase in C-O stretching frequency.[20] Theoretical studies on experimentally obtained $M^+-(CO)_n$ (M = Cu, Ag, Au) systems[19d-19f,20a,20d] show that significant σ donation from anti-bonding type HOMO of CO to M center and negligible π back donation from M to CO cause an increase in C-O stretching frequency compared to free CO. Recently, Frenking et al.[21] reported OCBeO and $OCBeCO_3$ complexes in which the C-O stretching frequency is larger than its normal gas phase value and termed them as 'non-classical' carbonyls.

Dissociation energy along with the thermochemical parameters like dissociation enthalpy (ΔH) and free energy change (ΔG) are evaluated to know the stability of the present systems. Energy decomposition analysis (EDA)[22] in conjuction with the natural orbitals for chemical valence (NOCV),[23] electron density and natural bond orbital (NBO) analyses are performed to explore the nature of interaction. There are many indicators to theoretically describe the magnetic properties of a system. Here, we have mainly used nucleus-independent chemical shift (NICS)[24] and its different extensions like zz-component of NICS tensor, $NICS_{zz}$,[25] NICS-rate[26]

and NICS in-plane component ($NICS_{in\text{-}plane}$) vs NICS out-of-plane ($NICS_{out\text{-}of\text{-}plane}$) component.[27] For M_3^+ systems, ring current maps are also generated.

Computational Details

The geometry optimization of the presently studied systems, except for the Ng bound analogues, is carried out with hybrid *meta*-GGA M06-2X functional of Zhao and Truhlar[28] in conjuction with the Ahlrichs' triple-ζ-quality basis set, def2-TZVP.[29] On the other hand, due to the weak interaction the Ng bound M_3^+ clusters are studied at the MP2/def2-TZVP level. A quasi-relativistic pseudopotential is used for Ag, Au, Xe and Rn atoms.[30] Harmonic vibrational frequencies are computed to characterize the nature of stationary points and to make the zero point vibrational energy (ZPE) corrections. The absence of imaginary frequency suggests that all the systems studied here correspond to the minima on the potential energy surface. Natural population analysis (NPA) is performed to compute the charge (q) at each atomic center. The correction from basis set superposition error (BSSE) is done by using the method proposed Boys and Bernardi.[31] Here, we have reported dissociation energy values (D_0^{BSSE}) corrected from both ZPE and BSSE. ΔH and ΔG are computed at 298 K and one atmospheric pressure. All these computations are done by using Gaussian 09 program package.[32] EDA-NOCV is performed at the PBE-D3/TZ2P taking the optimized geometries at the M06-2X/def2-TZVP or MP2/def2-TZVP level[33] using ADF2013.01 program package[34] and the scalar zero-order regular approximation (ZORA)[35] is considered for the heavier atoms. In EDA-NOCV, the total interaction energy (ΔE^{int}) is decomposed into physically meaningful terms as equation (1).

$$\Delta E^{int} = \Delta E^{Pauli} + \Delta E^{elstat} + \Delta E^{orb} + \Delta E^{disp} \tag{1}$$

In equation (1), Pauli repulsion (ΔE^{Pauli}) represents the repulsive Pauli interaction between the occupied orbitals of the interacting fragments; electrostatic term (ΔE^{elstat}) represents the classical electrostatic interactions between two fragments having the electron densities of the fragments at the frozen geometries that they have in the complex; orbital term (ΔE^{orb}) accounts for the interactions between occupied molecular orbitals of one fragment with the unoccupied molecular orbitals of another fragment, termed as charge transfer, as well as the mixing between empty and occupied orbitals on the same fragment, termed as polarization; and dispersion term (ΔE^{disp})

describes the dispersion interaction between two fragments. The EDA-NOCV scheme further decomposes the differential density ($\Delta\rho(r)$) into deformation densities ($\Delta\rho_i(r)$) and it represents the direction of flow of electron density. Corresponding to each $\Delta\rho_i(r)$ channel, ΔE^{orb} can also be decomposed into ΔE_i^{orb}.

The electron density analysis is performed at the M06-2X/def2-TZVP level (MP2/def2-TZVP level for Ng bound analogues) by using Multiwfn software.[36] Laplacian of the electron density ($\nabla^2\rho(r_c)$) is generally used to categorize a bond as covalent or noncovalent one. While a negative value at the bond critical point (BCP) implies electron density concentration, hence a covalent bond, a positive value indicates electron density depletion and therefore a noncovalent bond. But for the molecules involving heavier atoms or even for simple molecules, this criterion does not always work to represent a bond.[37] Cremer et al.,[38] thereafter, suggested that if the total energy density ($H(r_c)$) at the BCP is negative, the bond might be considered as of partial covalent type. $H(r_c)$ is the sum of local kinetic energy density ($G(r_c)$) and local potential energy density ($V(r_c)$).

NICS values are calculated at the M06-2X/def2-TZVP level of theory through the gauge-independent atomic orbital method (GIAO).[39] According to Schleyer's proposal,[24] NICS is the negative of the isotropic shielding constant (σ_{iso}) and equivalent to the induced magnetic field where the magnetic field is induced by the electrons of the molecule itself. There are several generally used NICS indices and NICS being a tensor, one can consider different components of the tensor as appropriate indices of aromaticity. NICS calculated at the ring center (NICS(0)) and 1 Å above the ring center (NICS(1)) are among the most used NICS indices. We have calculated NICS(0) by doping the dummy atom at the center of the ring and NICS(1) at 1 Å above the ring. Being a tensor, NICS can be decomposed into three components along the three coordinates as NICS = $-1/3(\sigma_{xx} + \sigma_{yy} + \sigma_{zz})$, where σ_{xx}, σ_{yy}, σ_{zz} are the isotropic shielding constants along x, y and z directions, respectively. Negative and positive NICS values of planar rings suggest aromaticity and antiaromaticity, respectively, whereas the near-zero values are associated with nonaromatic species. The 'perpendicular to the ring plane' components of NICS, $NICS_{zz}$ is known to give precise results towards predicting aromatic nature.[25] $NICS_{total}$ and $NICS_{zz}$ scans are performed from the ring center to 5 Å above of the ring center to obtain the additional information about the aromaticity of the studied systems. Recently, Tiznado et al.[27] calculated free of in-plane component NICS (FiPC-NICS) by plotting the $NICS_{in-plane}$ vs $NICS_{out-of-plane}$

components. If the molecule is aligned in xy plane and the z axis is perpendicular to the molecular plane then the previous component is described as, $NICS_{in\text{-}plane} = -1/3(\sigma_{xx} + \sigma_{yy})$ and the latter one, $NICS_{out\text{-}of\text{-}plane} = -1/3(\sigma_{zz})$. According to that study aromatic rings have negative $NICS_{out\text{-}of\text{-}plane}$ values and antiaromatic rings have positive $NICS_{out\text{-}of\text{-}plane}$ values. Previously Noorizadeh and Dardab[26] introduced the NICS-rate as an aromaticity index where the maximum/minimum in the NICS-rate curve ($\Delta NICS/\Delta r$ versus r) of a molecule indicates aromaticity/antiaromaticity of the system. NICS-rates are calculated from the difference between two successive NICS values. We have also applied the FiPC-NICS and NICS-rate approaches to verify the aromaticity in the studied systems. Multicenter bond indices (MBIs)[40] of M_3^+ clusters are further computed using Multiwfn software.[36] The MBI is used as an aromaticity descriptor[41] which is defined for the bonds involving A, B, C,······, L atoms as

$$MBI_{ABC\cdots L} = 2^L \sum_{a \in A,\, b \in B,\, \ldots,\, l \in L} \Pi_a^b \, \Pi_b^c \ldots \ldots \Pi_l^a \qquad (2)$$

where Π is an idempotent matrix.

Ring current density plots are generated with AIMAll software package.[42] The .wfx and .fchk files are generated from NMR calculations using the GIAO method[39] at the M06-2X/def2-TZVP level by the Gaussian 09 program package.[32] The molecules are placed in the xy plane and the magnetic field is applied in the –z direction (from the bottom side of the molecular plane).

σ-aromaticity in M_3^+

M_3^+ (M = Cu, Ag, Au) systems possess D_{3h} symmetry and $^1A_1'$ electronic state in their global minimum geometries (see Fig. 1).[43,8a] M_3^+ has 16 occupied molecular orbitals (MOs) and among which 15 MOs consist of d-atomic orbitals with bonding, nonbonding and antibonding types resulting in the net bonding effect zero.[43,8a] The a_1 highest occupied molecular orbital (HOMO) of M_3^+ is sum of ns-AOs of three M, which is σ-type and totally delocalized over M_3 unit (see Fig. 1-SI). Therefore, the HOMO corresponds to a three center-two electron (3c-3e) bond. In that sense they are similar to prototype σ-aromatic system, H_3^+ and its heavier congener, Li_3^+.[44] The M-M bond distance in M_3^+ is found to be slightly larger than those of the corresponding covalent bond distances.[45] The M-M bond distance ($r_{M\text{-}M}$) follows the order as $r_{Cu\text{-}Cu} < r_{Au\text{-}Au} < r_{Ag\text{-}Ag}$. The decreased $r_{Au\text{-}Au}$ value compared to $r_{Ag\text{-}Ag}$ is due to the fact that the

covalent radius of Au is around 0.1 Å less than that of Ag.[45] Very large relativistic effect in Au causes a contraction of valence 6s orbital followed by an expansion of inner 5d orbital which results in a reduced covalent radius.[46] The Wiberg bond index (WBI)[47] for M-M bond shows that almost half a covalent bond is formed therein. Consequently, $H(r_c)$ value at the BCP of M-M bond in M_3^+ is negative (-0.005 au for Cu-Cu, -0.004 au for Ag-Ag and -0.011 au for Au-Au bonds) supporting a partial covalent character.

Now, we have assessed the aromaticity of these M_3^+ clusters and compared with H_3^+ and Li_3^+ systems. It may be noted that there has a controversy regarding the aromaticity of Li_3^+. Although Li_3^+ has 2-delocalized σ-electrons and negative NICS values,[44b] Havenith et al.[48] termed Li_3^+ as nonaromatic based on its ring current map. The σ-aromaticity in all these M_3^+ molecules is indicated as the NICS$_{total}$–scan plots initially show large negative NICS value at the ring center (see Fig. 2a). Moreover, the NICS values gradually increase to zero upon the increased distance from the ring center. FiPC-NICS plots show that in these molecules in-plane components of the NICS are the maximum contributors towards the total aromaticity (see Fig. 2b). A single hump is found in NICS-rate plots for these molecules near the vicinity of ring center (< 0.7 Å) pointing towards the σ-aromaticity (see Fig. 2c). In can be noted that due to the small ring size of M_3^+ and the presence of d orbitals on M, NICS$_{zz}$–scan plots might be misleading. NICS–scan with only in–plane components predicts similar characteristics of these systems like NICS$_{total}$–scan. Among these triatomic cationic rings, H_3^+ shows the maximum σ-aromaticity, being the smallest molecule. On the other hand, M_3^+ is significantly more aromatic than Li_3^+. Upon the increased distance from the center, NICS value falls very sharply in case of H_3^+; however, in M_3^+ it falls much slowly. Furthermore, on applying a magnetic field perpendicular to the plane of the ring, it can induce a current density in and parallel to the molecular plane. An aromatic species is identified with the diatropic ring current circulating over the ring frame. In H_3^+, Cu_3^+, Ag_3^+ and Au_3^+, the diatropic ring current circulates around the molecular ring. However, in case of Li_3^+, similar to the results of Havenith et al.[48] only local diatropic ring circulates over the atoms but lacks any global circulation within the plane of the ring (see Fig. 3). Therefore, in H_3^+ and M_3^+ the HOMO electrons contribute global circulation whereas the same in Li_3^+ contribute a local circulation. This observation confirms the aromaticity in M_3^+ systems. MBI, which is known to be another descriptor of aromaticity,[41] is generally high

for aromatic systems whereas it is quite small in antiaromatic systems. The related values depend on the size of the ring. While in H_3^+ MBI was reported as 0.222,[41a] in five- and six-membered aromatic rings it varies in the 10^{-2} order.[41b] In our cases, MBIs in M_3^+ show quite similar values (0.284 in Cu_3^+, 0.282 in Ag_3^+, 0.230 in Au_3^+) to that in H_3^+ (0.296) at the same level confirming the presence of a 3c-2e bond.

Yong and coworkers[43] computed the resonance energy (RE) in Cu_3^+ due to σ-aromaticity by following the reaction as

$$Cu_3Cl\ (C_{2v},\ ^1A_1) \rightarrow Cu_2\ (D_{\infty h},\ ^1\textstyle\sum_g) + CuCl\ (C_{\infty v},\ ^1\textstyle\sum) \tag{3}$$

Previously, Alexandrova and Boldyrev[44b] also used a similar reaction to compute RE in Li_3^+. The RE values following the above reaction in M_3^+ cases are found to be 41.0, 35.5 and 24.4 kcal/mol in Cu_3^+, Ag_3^+ and Au_3^+, respectively.

NHC, pyridine, isoxazole and furan bound M_3^+

Owing to cationic charge, the electron affinity (EA) of M_3^+ is large ranging from 6.43-7.52 eV reflecting their large attraction towards an electron and, hence, towards a nucleophile. Therefore, suitable ligands are needed to stabilize them. Robilotto et al.[16] found that NHC bound Au_3^+ is relatively inert compared to bare Au_3^+ with larger energy gap between the HOMO and the lowest unoccupied molecular orbital (LUMO). The crystal structure of $(NHC)_3Au_3^+$ roughly corresponds to a D_3 point group. Here, in addition to $(NHC)_3Au_3^+$, we have considered $(NHC)_3Cu_3^+$ and $(NHC)_3Ag_3^+$. Similar to Au analogue, though both of them adopt D_3 symmetry, a slight structural difference is found in Cu analogue from those of Ag and Au complexes. Unlike the latter ones in the former complex, the imidazolylidene rings of NHC link with Cu centers in a tilted manner (see **1** in Fig. 1). The similar geometry for Cu as those of Ag and Au analogues (**2**) is 1.1 kcal/mol (including ZPE correction) higher in energy than **1**. On the other hand, $M_3(Py)_3^+$, $M_3(IOZ)_3^+$ and $M_3(Fu)_3^+$ correspond to D_3, C_{3v} and C_3 point groups, respectively, with equal M-M and M-Ligand(L) bond distances, except for the $Au_3(IOZ)_3^+$ case (see Fig. 1). One Au-Au bond in Au_3 fragment of the latter complex gets a little bit squeezed (by 0.003 Å) compared to other two bonds forming an isosceles triangle and the overall complex adopts a C_s

point group. For all these complexes, we have searched for a possible number of structures. The other structures are either higher energy minima or they possess imaginary frequency. The related results of the studied complexes are provided in Table 1. It may be noted that all the ligands reduce EA of M_3^+ significantly. Except in $Cu_3(NHC)_3^+$, HOMO-LUMO energy gap is also found to be larger in $M_3(L)_3^+$ than those in bare clusters reflecting larger electronic stability in former ones. D_0^{BSSE} values per L reveal that NHC ligand forms the strongest bond with M_3^+ followed by Py, IOZ and Fu. For a given L, it follows the order as $Au_3(L)_3^+ > Cu_3(L)_3^+ > Ag_3(L)_3^+$, except for the Fu case for which D_0^{BSSE} value is slightly larger in $Cu_3(Fu)_3^+$ than that in Au analogue. Corresponding ΔH and ΔG values also follow the same order as that of D_0^{BSSE}. Note that the dissociation processes producing 3L and M_3^+ are endergonic in nature at room temperature and one atmospheric pressure, for all cases. Upon coordination with different L, the r_{M-M} values get changed only slightly (< 0.04 Å) compared to those in M_3^+. For a given L, the bonding distance between M and the binding site of L (r_{M-L}) follows the order as $r_{Cu-L} < r_{Au-L} < r_{Ag-L}$.

There is a degree of net electron transfer from L to M center resulting in a decrease in positive charge of M. Such electron transfer is found to be maximum for NHC and minimum for Fu whereas it is almost same for Py and IOZ. Being a carbene, NHC would be obviously the best electron donor. As O center in Fu is more electronegative than those of N centers of Py and IOZ, the electron transfer is less in former one. The WBI values corresponding to M-L bonds are largest in case of NHC among the other ligands. It indicates that the M-C bonds in $M_3(NHC)_3^+$ are most covalent one among the other M-L bonds under consideration. It may also be noted that the degree of covalency in Au-C bond is larger than those in Cu-C and Ag-C bonds in $M_3(NHC)_3^+$ as indicated by the respective WBI values. In fact, for a given L it follows the order as $WBI_{Au-L} > WBI_{Cu-L} > WBI_{Ag-L}$ in all cases. The electron density analysis shows that $\nabla^2\rho(r_c)$ is positive at BCPs either in M-L bonds or in M-M bonds; however, $H(r_c)$ values are negative reflecting the partial covalent character (see Table 2). Upon coordination with L, the $H(r_c)$ values become slightly more negative for M-M bonds compared to those in M_3^+. For a given M, the negative value of $H(r_c)$ is larger in M-C bonds of $M_3(NHC)_3^+$ than the other L bound complexes. It supports the argument regarding the larger covalency in M-C bonds compared to the other M-L bonds. Apart from that in case of $Cu_3(Fu)_3^+$, $H(r_c)$ value is only slightly more negative than

that in $Au_3(Fu)_3^+$, similar to order of WBI, $H(r_c)$ also follows the same order in moving from Cu to Au for same L.

Now, to obtain more insight into the bonding situation let us look at the EDA-NOCV results performed considering L as one fragment and $M_3L_2^+$ as another fragment (see Table 3). ΔE^{int} is the energy difference between L-bound system and the sum of its fragment energies restricting to the same geometry constrained to that of L-bound complexes. For all cases, the contribution from ΔE^{elstat} is maximum (*ca.* 58-71%) towards the total attraction whereas ΔE^{orb} contributes around 26-36% of total attraction. ΔE^{disp} contributes negligibly. Similar to the degree of electron transfer, the C center in NHC makes the largest orbital interaction with M among the other L whereas O center in Fu makes the smallest orbital interaction with M. It may also be noted that for a given L, the orbital interaction follows the same order as that of WBI i.e., $Au_3(L)_3^+ > Cu_3(L)_3^+ > Ag_3(L)_3^+$. The plots of the $\Delta\rho(r)$ for $M_3(NHC)_3^+$ and $M_3(Py)_3^+$ are displayed in Fig. 4 (the corresponding results for $M_3(IOZ)_3^+$ and $M_3(Fu)_3^+$ are given in Fig. 2-SI). It is found that both L→M electron donation and L←M electron back donation contribute towards the total ΔE^{orb}. ΔE_1^{orb} corresponds to L→M σ donation and this is responsible for 54-69% of total ΔE^{orb}. In the plot, the electron density shifts from red to blue. $\Delta\rho_1(r)$ in Fig. 4 shows the electron density is shifted from L to attached M center and from which it is further transferred to the adjacent M centers. On the other hand, $\Delta\rho_n(r)$ (n = 2, 3, 4) corresponds to the L←M electron back donation, $\Delta\rho_2(r)$ and $\Delta\rho_4(r)$ being π type back donation and $\Delta\rho_3(r)$ being σ type back donation. The associated ΔE_i^{orb} values with these $\Delta\rho_n(r)$ reveal that L←M back donation contributes around 31-36% of total ΔE^{orb}. Note that ΔE_1^{orb} corresponding to L→M σ donation follows the same order as those of ΔE^{int} and/or D_0^{BSSE} values, either for a given M with different L or for a given L with different M. However, the ability to accept electron via L←M back donation is found to be the highest for NHC ligand among others following the order as NHC > IOZ > Py > Fu, for a given M.

$NICS_{total}$–scan plots show that, in general all the L bound M_3^+ complexes show more aromatic nature compare to the bare M_3^+ species (see Fig. 5). The increase in aromaticity is even more significant in $Au_3L_3^+$ complexes. However, in comparison to the recently studied $Zn_3Cp^*_3^+,[18]$ the present $M_3L_3^+$ (M = Cu, Ag) complexes show somewhat less aromaticity than the former one whereas aromaticity in $Au_3L_3^+$ (L = Py, IOZ, Fu) complexes is very close to that

in Zn_3 complex. FiPC-NICS scan (see Fig. 3-SI) and NICS-rate plots (see Fig. 4-SI) also verify the similar characteristics as found in $NICS_{total}$–scan plots.

Noble gas bound M_3^+

Similar to bare M_3^+, $M_3Ng_3^+$ complexes possess a D_{3h} symmetry and $^1A_1'$ electronic state (see Fig. 6). By symmetry, each of the M centers in any M_3^+ possesses an equal amount of charge of + 0.33 $|e|$. It is found that M_3^+ clusters can form stable Ng compounds.[49] D_0^{BSSE} values per Ng atom are 3.9 (Cu), 2.2 (Ag) and 5.4 (Au) kcal/mol for Ar, 6.4 (Cu), 3.9 (Ag), and 9.8 (Au) kcal/mol for Kr, 9.6 (Cu), 6.5 (Ag) and 15.9 (Au) kcal/mol for Xe, and 11.2 (Cu), 8.1 (Ag) and 19.0 (Au) kcal/mol for Rn (see Table 4). Therefore, for a given Ng, the Ng binding ability of M_3^+ follows the order as $Au_3^+ > Cu_3^+ > Ag_3^+$. On the other hand, for a given M, the stability of the Ng bound M_3^+ complexes gradually increases in moving from Ar to Rn. The increase in polarizability of Ng along the same is presumably the reason for this observation. All the dissociation processes are endothermic in nature and the corresponding ΔH values also follow the same trend as that of D_0^{BSSE} either upon moving from Cu to Au or along Ar to Rn. It may be noted that formation of both M_3Ng^+ and $M_3Ng_2^+$ will also be feasible in experimental situation. But, since Shayeghi et al. observed that the intensity of $Au_3Ar_3^+$ is larger than the other smaller complexes in mass spectrum, here we have only considered tri-Ng bound analogues. Quite small D_0^{BSSE} value in case of $Ag_3Ar_3^+$ supports the fact that Shayeghi et al.[17] obtained very small peak for $Ag_3Ar_n^+$ (n =1, 2, 3) in mass spectrum. Nevertheless, if one considers the heavier congeners of Ar, the corresponding Ng bound analogues are more likely to be formed. Except for $Cu_3Ar_3^+$, $Ag_3Ar_3^+$ and $Ag_3Kr_3^+$ cases, the dissociation processes of the rest of the systems are found to be endergonic in nature at room temperature and one atmospheric pressure. Computation of the HOMO-LUMO energy gap implies that HOMO-LUMO energy gap improves upon Ng binding compared to the bare clusters indicating their increased electronic stability (see Table 4). The electron affinity of M_3^+ also decreases in Ng bound analogues.

On analyzing NPA charge values we have found a loss of positive charge on M center and a development of positive charge on Ng atom concurrently, which illustrates the degree of electron transfer from Ng to M. The amount of charge transfer from Ng to M center is lower for

lighter Ng atoms and it consistently increases with shifting toward heavier one. Owing to the variation in polarizability this trend is expected. The WBI values range from 0.11 to 0.26 for $Cu_3Ng_3^+$, 0.08 to 0.23 for $Ag_3Ng_3^+$, and 0.14 to 0.35 for $Au_3Ng_3^+$ with gradual increase in moving from Ar to Rn. For a given Ng, bond length of Ng-Cu is the shortest and is the longest for Ng-Ag following the order as Cu-Ng < Au-Ng < Ag-Ng. Upon Ng binding, the M-M bond distances get slightly shortened compared to those in the free M_3^+.

The results of the EDA taking Ng as one fragment and $M_3Ng_2^+$ as another fragment are provided in Table 5. Among the attractive terms, while the contributions from ΔE^{orb} (*ca*. 43-53%) and ΔE^{elstat} (*ca*. 42-56%) terms are found to be almost equal towards the total attraction, the contribution from ΔE^{disp} term is negligible towards the same. Therefore, the M-Ng bonds in $M_3Ng_3^+$ may be considered as a mixture between electrostatic interaction and covalent interaction. This is very similar to those in Ng-M bonds in NgMX (X = F, Cl, Br) or NgMCN.[50] The plot of $\Delta\rho(r)$ is provided in Fig. 7 and the associated ΔE_i^{orb} values are also mentioned. It is found that electron density is accumulated in between M and Ng centers. This observation is quite similar to those of the studies on NgAuF and $NgAu^+$ by Belpassi et al.[51] and on NgMCN by Pan et al.[50i] The corresponding ΔE_i^{orb} value associated with this accumulation of electron density gradually increases along Ar to Rn indicating larger covalent contribution along the same.

The results of electron density analysis reveal that though $\nabla^2\rho(r_c)$ is found to be positive in all cases, except for the Ag-Ar bond $H(r_c)$ is negative for all other bonds implying the partial covalent character (see Table 6). It may be noted that the corresponding M-Ng bond distances become quite close to those of the typical M-Ng covalent bond distances (r_{cov}) for Xe and Rn cases. In Ng bound analogues, the negative values of $H(r_c)$ only get slightly increased in M-M bonds compared to the bare clusters.

The change in aromaticity upon the binding with Ng atoms is studied and the related results are provided in the supporting information (see Figs. 5-SI, 6-SI and 7-SI). It is found that $M_3Ng_3^+$ complexes are slightly more aromatic in comparison to the M_3^+.

Carbon monoxide bound M_3^+

The optimized geometries of $M_3(CO)_3^+$ and $M_3(OC)_3^+$ along with their geometrical parameters are provided in Fig. 8. All the structures correspond to D_{3h} point group and $^1A_1'$ electronic state. While the C-O bond distance in $M_3(CO)_3^+$ gets decreased compared to that in the free CO, the C-O bond distance becomes longer in $M_3(OC)_3^+$. In cases of $Cu_3(CO)_3^+$ and $Ag_3(CO)_3^+$, C-O bond becomes shorter by 0.008 Å than that in free CO whereas in $Au_3(CO)_3^+$ C-O bond gets slightly less shorter (0.007 Å) compared to others. On the other hand, the C-O bond distances in $M_3(OC)_3^+$ undergo gradually larger lengthening in moving from Ag (0.007 Å) to Au (0.008 Å) to Cu (0.009 Å). The computed D_0^{BSSE} value per CO in $M_3(CO)_3^+$ is by 10.4 kcal/mol for Cu, 7.7 kcal/mol for Ag and 17.4 kcal/mol for Au larger than that in $M_3(OC)_3^+$ depicting the larger stability of the former isomer than that of the latter (see Table 7). For $M_3(CO)_3^+$, D_0^{BSSE} value follows the order as $Au_3(CO)_3^+ > Cu_3(CO)_3^+ > Ag_3(CO)_3^+$ whereas for $M_3(OC)_3^+$ the order becomes $Cu_3(CO)_3^+ > Au_3(CO)_3^+ > Ag_3(CO)_3^+$. The computed ΔH and ΔG values for the dissociation process of the respective complexes also follow that order. Now, a very interesting aspect would be the vibrational frequency corresponding to the C-O stretching mode. The C-O stretching frequency of free CO at the studied level of theory is 2269 cm^{-1}. For all the three sets, $M_3(CO)_3^+$ has a blue-shifted C-O stretching frequency ($\Delta\nu_{CO} > 0$) whereas $M_3(OC)_3^+$ exhibits a red-shifted C-O stretching frequency ($\Delta\nu_{CO} < 0$). By symmetry, there are two types of C-O stretching mode, one being doubly degenerate IR active asymmetric stretching mode (E′) and another being IR inactive symmetric stretching mode (A_1'). The ν_{CO} corresponding to A_1' is slightly larger than that of E′ (see Table 7). The blue-shift is largest in $Cu_3(CO)_3^+$ following the order as $Cu_3(CO)_3^+ > Ag_3(CO)_3^+ > Au_3(CO)_3^+$ whereas in case of red-shift, the order is $Cu_3(CO)_3^+ > Au_3(CO)_3^+ > Ag_3(CO)_3^+$. It follows the same order as those of C-O bond shortening and elongation. It may be noted that though CO is more strongly bonded with Au_3^+ than Cu_3^+, $\Delta\nu_{CO}$ is higher in latter complex than that in the former.

To inspect this reason and to get a detail insight into the bonding situation of this donor-acceptor interaction, the results of EDA-NOCV is analyzed (see Table 8). In both C-side and O-side binding, the contribution from ΔE^{elstat} (*ca.* 51-62 %) is found to be larger than that of ΔE^{orb} (*ca.* 37-46 %). The stronger Au-CO bond than Cu-CO bond can be attributed to the larger orbital and electrostatic interactions in $Au_3(CO)_3^+$ than that in $Cu_3(CO)_3^+$. It is well-known that OC→M σ donation tends to increase the ν_{CO} whereas M→CO π back bonding is responsible for the

lowering of ν_{CO}. The explanation for the latter observation is quite straightforward. As it populates the antibonding π^* orbital, it causes a lengthening of C-O bond length accompanied by a red shift in ν_{CO}. However, the reason for the former observation involves a confusion for a long time. Initially, it was argued that the HOMO of CO, which is a σ-orbital, possesses an antibonding character.[52] The shorter C-O bond length and higher ν_{CO} in CO^+ and HCO^+ supports this argument.[53] However, the shape of HOMO and significant red-shift in ν_{CO} in COH^+ opposes the antibonding concept of HOMO.[54] Frenking et al.[20d] explained this in terms of an opposing polarization in the σ- and π-orbitals upon bonding with H^+ or M^+ through either end of CO. In free CO, the bonding orbitals remain polarized towards more electronegative O-end. Therefore, a positive charge at the C-end will attract the electron density from O-end resulting in a less polarized bond and hence a more covalent bond. On the other hand, a positive charge attached with O-end results in a more polarized bond and hence a larger C-O bond distance.

As Frenking and coworkers[19k] mentioned, there are two possible situations for being $\Delta\nu_{CO} > 0$: 1) relatively low M $\rightarrow$ CO π back bonding or 2) π back donation is significant but not large enough to overbalance the σ donation. It was also observed that a small degree of π back donation is enough to overshadow the σ donation resulting in a larger C-O bond length.[20a-20c] An inspection of σ- and π-contributions towards ΔE^{orb} reveals that the $OC \rightarrow M_3(CO)_2^+$ σ donation is 14.3 kcal/mol larger in $Au_3(CO)_3^+$ than that in $Cu_3(CO)_3^+$. However, at the same time $OC \leftarrow M_3(CO)_2^+$ π back donation is 9.7 kcal/mol higher in former species than that in the latter one. Therefore, larger π back donation is responsible for the lower ν_{CO} in $Au_3(CO)_3^+$ compared to $Cu_3(CO)_3^+$. In case of $Ag_3(CO)_3^+$, though σ donation is less by 3.7 kcal/mol than $Cu_3(CO)_3^+$, the π back donation is also lower by 5.4 kcal/mol resulting in a ν_{CO} in $Ag_3(CO)_3^+$ very close to that in $Cu_3(CO)_3^+$. Now, in cases of $M_3(OC)_3^+$ both the σ donation and π back donation are relatively low compared to those in $M_3(CO)_3^+$ isomer. One way to explain the red-shift in ν_{CO} in these complexes is that due to poor σ donation, the π back donation becomes large enough to cause a red-shift in ν_{CO}. It may also be noted that the relative amount of red-shift in ν_{CO} follows the same order as that of π back donation.

Let us check the alternative explanation[20d] of opposing polarization in the σ- and π-orbitals to describe these observations. The computed partial charges on C and O centers imply

that in C-side bonding the lone-pair donation from C center is compensated by the electron redistribution within CO fragment and as a result the negative charge on O decreases. It may also be noted that the charge separation in free CO is $1.00 \, |e|$ which decreases to some extent in C-side bonding of CO. On the other hand, in cases of O-side bonding the electron donation from O center of CO is even overcompensated by the induced polarization within CO resulting in more negatively charged O center and more positively charged C center than those in free CO. Consequently, it increases the overall polarization within CO (charge separation more than $1.00 |e|$). This is the reason why the WBI value for M-C bond is considerably larger than that for M-O bond. Therefore, the present results support the argument of opposing polarization.[20d] Note that larger the charge separation within CO, larger the red-shift is found. Fig. 9 displays $\Delta\rho$ corresponding to σ donation and π back donation. The shape of $\Delta\rho(\sigma)$ shows that though the electron donation mainly takes place from C or O centers of CO for C-side or O-side binding, respectively, the electronic charge at the other end also gets depleted as indicated by the red color. The plot of $\Delta\rho(\pi)$ also shows that in C-side and O side bonding the π back donation only leads to the electron accumulation at the C and O centers of CO, respectively, whereas the electron density from the other end of CO also comes to the binding end. It supports the induced polarization occurred with CO moiety as obtained from NPA charge. There also exists another orbital pair, which is related to the polarization of C-O σ-bond ($\Delta\rho(pol)$). HOMO-LUMO energy gap is found to be significantly improved in CO bound analogues compared to the bare clusters.

$H(r_c)$ values corresponding to the M-C bonds in $M_3(CO)_3^+$ isomers are considerably more negative than those of the M-O bonds in $M_3(OC)_3^+$ (see Table 9). It shows that the former bonds are more covalent in nature than the latter ones supporting the corresponding WBI values. Nevertheless, upon CO binding $H(r_c)$ values of M-M bonds also become slightly more negative than those in free M_3^+.

Similar to the other ligand bound complexes, CO and OC bound M_3^+ complexes are also found to be more aromatic in comparison to the unbound M_3^+ clusters (see Figs. 5-SI, 6-SI and 7-SI).

Summary and conclusions

Because of the fact that the HOMO comprises the sum of ns-AOs of three M, M_3^+ (M = Cu, Ag, Au) is a σ-aromatic system. Nucleus-independent chemical shift (NICS) and its different extensions like NICS-rate and NICS in-plane component ($NICS_{in\text{-}plane}$) vs NICS out-of-plane ($NICS_{out\text{-}of\text{-}plane}$) component are computed to assess aromaticity. The aromaticity in Au_3^+ is somewhat higher than that of Cu_3^+ and Ag_3^+. A comparison with Li_3^+ and prototype σ-aromatic system, H_3^+ reveals that M_3^+ clusters have lower aromaticity than that of H_3^+ but have significantly higher aromaticity with respect to Li_3^+. Almost half a covalent bond occurs in M-M bonds of M_3^+ as indicated by the Wiberg bond index (WBI) values of ~0.5 and negative values of total energy density ($H(r_c)$). Different ligands like N-heterocyclic carbene (NHC), dimethyl imidazol-2-ylidene, pyridine (Py), isoxazole (IOZ), furan (Fu), noble gas (Ng) and carbon monoxide (CO) can bind with these M_3^+ clusters with favorable interaction. They lower the high electron affinity of M_3^+ and in general increases the energy gap between the highest occupied molecular orbital and the lowest unoccupied molecular orbital. Among the ligands, NHC, Py, IOZ and Fu, NHC forms the strongest bond with M_3^+ followed by Py, IOZ and Fu. On the other hand, in general the dissociation energy per ligand (L) follows the order as $Au_3(L)_3^+ > Cu_3(L)_3^+ > Ag_3(L)_3^+$, for a given L. Because of the smaller covalent radius of Au than that of Ag, the bonding distance between M and the binding site of a given L ($r_{M\text{-}L}$) follows the order as $r_{Cu\text{-}L} < r_{Au\text{-}L} < r_{Ag\text{-}L}$. Energy decomposition analysis in conjuction with the natural orbitals for chemical valence (EDA-NOCV) show that electrostatic contribution (ΔE^{elstat}) is maximum (*ca*. 58-71%) towards the total attraction in M-L bonds. On the other hand, orbital contribution (ΔE^{orb}) is around 26-36% of total attraction. Both L→M σ donation (*ca*. 54-69%) and L←M back donation (*ca*. 31-36%) contribute towards the total ΔE^{orb}. The negative $H(r_c)$ values in M-L bonds imply the partial covalent character therein. Upon bonding with L, the aromaticity within M_3 moiety increases compared to the bare M_3^+ clusters. However, Zn_3 moiety in the recently synthesized[18] $Zn_3Cp*_3^+$ is somewhat more aromatic than those in $M_3(L)_3^+$ (M = Cu, Ag). The aromaticity in $Au_3L_3^+$ (L = Py, IOZ, Fu) complexes is quite comparable with that in Zn_3 complex.

M_3^+ clusters can bind Ng atoms quite effectively. For a given Ng, the Ng binding ability of M_3^+ follows the order as $Au_3^+ > Cu_3^+ > Ag_3^+$. The Ng dissociation process is endergonic in nature at room temperature and one atmospheric pressure, except for $Cu_3Ar_3^+$, $Ag_3Ar_3^+$ and $Ag_3Kr_3^+$. In M-Ng bond, the contribution from ΔE^{orb} and ΔE^{elstat} terms are almost equal towards

the attraction energy. Except for the Ag-Ar bond, the other M-Ng bonds are found to be of partial covalent type as indicated by the negative $H(r_c)$ values. $M_3Ng_3^+$ complexes are slightly more aromatic than M_3^+.

Further, the structure and stability of $M_3(CO)_3^+$ and $M_3(OC)_3^+$ are analyzed. Bonding through the C-end of CO is much more favorable than that of the O-end bonding. While for C-side bonding, the CO binding ability of M_3^+ follows the order as $Au_3^+ > Cu_3^+ > Ag_3^+$, for O-side bonding the order is $Cu_3^+ > Au_3^+ > Ag_3^+$. In $M_3(CO)_3^+$, a blue-shifted C-O stretching frequency is found whereas in $M_3(OC)_3^+$ a red-shift in C-O stretching frequency occurs. These observations can be explained by the reverse polarization of the σ- and π-orbitals of CO as well as the relative amount of OC→M σ donation and M→CO π back donation. The blue-shift and the red-shift are largest in $Cu_3(CO)_3^+$ and $Cu_3(OC)_3^+$, respectively. Despite the stronger Au-C bond in $Au_3(CO)_3^+$, larger Au→CO π back bonding is responsible for lowering of the C-O stretching frequency compared to that in $Cu_3(CO)_3^+$. The bonding with CO increases the aromaticity of M_3^+ to some extent.

Acknowledgements

References

1. http://www.rsc.org/chemistryworld/2015/01/what-we-mean-when-we-talk-about-bonds (Last accessed 13/10/2015)
2. A. W. Hofmann, *Proc. R. Soc.*, 1855, **8**, 1.
3. A. Kekulé, *Bull. Soc. Chim. Fr.* (Paris), 1865, **3**, 98.
4. J. Dewar, *Proc. R. Soc. Edinburgh*, 1867, **6**, 82.
5. W. Armit and R. Robinson, *J. Chem. Soc. Trans.*, 1925, **127**, 1604.

6. a) W. Heitler and F. London, *Z. Phys*., 1927, **44**, 455; b) L. Pauling and G. W. Wheland, *J. Chem. Phys*., 1933, **1**, 280; c) L. Pauling, *J. Chem. Phys*., 1936, **4**, 673.

7. E. Hückel, *Z Phys*., 1931, **70**, 204.

8. a) D. Y. Zubarev, B. B. Averkiev, H.-J. Zhai, L.-S. Wang and A. I. Boldyrev, *Phys. Chem. Chem. Phys*., 2008, **10**, 257; b) R. B. King, *Chem. Rev*., 2001, **101**, 1119; c) A. Hirsch, Z. Chen and H. Jiao, *Angew. Chem. Int. Ed*., 2000, **39**, 3915; d) M. Bühl and A. Hirsch, *Chem. Rev*., 2001, **101**, 1153; e) J. Poater and M. Solà, *Chem. Commun*., 2011, **47**, 11647.

9. a) X. Li, A. E. Kuznetsov, H. -F. Zhang, A. I. Boldyrev and L. S. Wang, *Science*, 2001, **291**, 859; b) A. Kuznetsov, K. Birch, A. I. Boldyrev, X. Li, H. Zhai and L. S. Wang, *Science*, 2003, **300**, 622.

10. a) A. C. Tsipis and C. A. Tsipis, *J. Am. Chem. Soc*., 2003, **125**, 1136; b) C. A. Tsipis, E. E. Karagiannis, P. F. Kladou and A. C. Tsipis, *J. Am. Chem. Soc*., 2004, **126**, 12916; c) A. C. Tsipis and C. A. Tsipis, *J. Am. Chem. Soc*., 2005, **127**, 10623; d) A. C. Tsipis and A. V. Stalikas, *New J. Chem*., 2007, **31**, 852; e) H. Tanaka, S. Neukermans, E. Janssens, R. E. Silverans and P. Lievens, *J. Am. Chem. Soc*., 2003, **125**, 2862; f) C. S. Wannere, C. Corminboeuf, Z.-X. Wang, M. D. Wodrich, R. B. King and P. v. R. Schleyer, *J. Am. Chem. Soc*., 2005, **127**, 5701; g) Y.-C. Lin, D. Sundholm, J. Juselius, L.-F. Cui, X. Li, H. J. Zhai and L. S. Wang, *J. Phys. Chem. A*, 2006, **110**, 4244; h) A. E. Kuznetsov, J. D. Corbett, L.-S. Wang and A. I. Boldyrev, *Angew. Chem., Int. Ed*., 2001, **40**, 3369; i) L. Yong and C. Chi, *J. Mol. Struct*., 2007, **818**, 93; j) X. X. Chi and Y. Liu, *Int. J. Quantum Chem.*, 2007, **107**, 1886; k) X. Huang, H. J. Zhai, B. Kiran and L. S. Wang, *Angew. Chem., Int. Ed.*, 2005, **44**, 7251; l) H. J. Zhai, B. B. Averkiev, D. Yu. Zubarev, L. S. Wang and A. I. Boldyrev, *Angew. Chem., Int. Ed*., 2007, **46**, 4277; m) B. B. Averkiev and A. I. Boldyrev, *J. Phys. Chem. A*, 2007, **111**, 12864; n) P. K. Chattaraj and S. Giri, *J. Mol. Struct*., 2008, **865**, 53; o) A. I. Boldyrev and L. S. Wang, *Chem. Rev*., 2005, **105**, 3716; p) C. A. Tsipis, *Coord. Chem. Rev*., 2005, **249**, 2740; q) "Aromaticity and Metal Clusters" ed. P. K. Chattaraj, Taylor & Francis/CRC Press, Boca Raton, New York (2011) ISBN: 9781439813348; r) F. Feixas, E. Matito, J. Poater and M. Solà, *WIREs Comput. Mol. Sci*., 2013, **3**, 105.

11. R. Hoffmann, *Am. Sci*., 2015, **103**, 18.

12. A. I. Boldyrev and L.-S. Wang, *Chem. & Eng. News*, 2015, http://cen.acs.org/articles/93/i8/Aromaticity1.html

13. a) M. A. Omary, M. A. Rawashdeh-Omary, M. W. A. Gonser, O. Elbjeirami, T. Grimes, T. R. Cundari, H. V. K. Diyabalanage, C. S. P. Gamage and H. V. R. Dias, *Inorg. Chem*., 2005, **44**, 8200; b) L. Hou, W.-J. Shi, Y.-Y. Wang, H.-H. Wang, L. Cui, P.-X. Chen and Q.-Z. Shi, *Inorg. Chem*., 2011, **50**, 261; c) A. Burini, A. A. Mohamed and J. P. Fackler, *Inorg. Chem. Commun*., 2003, **24**, 253; d) A. A. Mohamed, J. M. Lòpez-de Luzuriaga and J. P. J. Fackler, *J. Cluster Sci*., 2003, **14**, 61; e) A. A. Mohamed, A. Burini and J. P. Fackler, *J. Am. Chem. Soc*., 2005, **127**, 5012; f) A. A. Mohamed, R. Galassi, F. Papa, A. Burini and J. P. Fackler, *Inorg. Chem*., 2006, **45**, 7770; g) A. A. Mohamed, L. M. Prez and J. P. Fackler Jr., *Inorg. Chim. Acta*, 2005, **358**, 1657; h) M. A. Omary, A. A. Mohamed, M. A. Rawashdeh-Omary and J. P. Fackler Jr., *Coord. Chem. Rev*., 2005, **249**, 1372; i) H. V. R. Dias and C. Palehepitiya Gamage, *Angew. Chem., Int. Ed*., 2007, **46**, 2192; j) H. V. R. Dias, S. Singh and C. F. Campana, *Inorg. Chem*., 2008, **47**, 3943; k) J.-P. Zhang and S. Kitagawa, *J. Am. Chem. Soc*., 2008, **130**, 907; l) S. M. Tekarli, T. R. Cundari and M. A. Omary, *J. Am. Chem. Soc*., 2008, **130**, 1669; m) H. V. R. Dias, C. S. P. Gamage, J. Keltner, H. V. K. Diyabalanage, I. Omari, Y. Eyobo, N. R. Dias, N. Roehr, L.

McKinney and T. Poth, *Inorg. Chem*., 2007, **46**, 2979; m) A. A. Titov, O. A. Filippov, A. N. Bilyachenko, A. F. Smol'yakov, F. M. Dolgushin, V. K. Belsky, I. A. Godovikov, L. M. Epstein and E. S. Shubina, *Eur. J. Inorg. Chem*., 2012, **2012**, 5554; n) G. Yang, P. Baran, A. R. Martínez and R. G. Raptis, *Cryst. Growth Des*., 2013, **13**, 264; o) S.-Z. Zhan, M. Li, S. W. Ng and D. Li, *Chem. – Eur. J*., 2013, **19**, 10217.

14. L. G. Vaughan, *J. Am. Chem. Soc*., 1970, **92**, 730.

15. G. F. Caramori, R. M. Piccoli, M. Segala, A. Muñoz-Castro, R. Guajardo-Maturana, D. M. Andrada and G. Frenking, *Dalton Trans*., 2015, **44**, 377.

16. T. J. Robilotto, J. Bacsa, T. G. Gray and J. P. Sadighi, *Angew. Chem. Int. Ed*., 2012, **51**, 12077.

17. A. Shayeghi, R. L. Johnston, D. M. Rayner, R. Schäfer and A. Fielicke, *Angew. Chem., Int. Ed*., 2015, **54**, 10675.

18. K. Freitag, C. Gemel, P. Jerabek, I. M. Oppel, R. W. Seidel, G. Frenking, H. Banh, K. Dilchert and R. A. Fischer, *Angew. Chem. Int. Ed*., 2015, **54**, 4370.

19. a) S. H. Strauss, *Chemtracts: Inorg. Chem*., 1997, **10**, 77; b) J. E. Ellis and W. Beck, *Angew. Chem. Int. Ed*., 1995, **34**, 2489; c) L. Weber, *Angew. Chem. Int. Ed*., 1994, **33**, 1077; c) F. Aubke and C. Wang, *Coord. Chem. Rev*., 1994, **137**, 483; d) J. J. Rack, J. D. Webb and S. H. Strauss, *Inorg. Chem*., 1996, **35**, 277; e) P. K. Hurlburt, J. J. Rack, J. S. Luck, S. F. Dec, J. D. Webb, O. P. Anderson and S. H. Strauss, *J. Am. Chem. Soc*., 1994, **116**, 10003; f) H. Willner, J. Schaebs, G. Hwang, F. Mistry, R. Jones, J. Trotter and F. Aubke, *J. Am. Chem. Soc*., 1992, **114**, 8972; g) H. Willner, M. Bodenbinder, C. Wang and F. Aubke, *J. Chem. Soc. Chem. Commun*., 1994, 1189; h) C. Bach, H. Willner, C.Wang, S. J. Rettig, J. Trotter and F. Aubke, *Angew. Chem. Int. Ed*., 1996, **35**, 1974; i) C. D. Desjardins, D. B. Edwards and J. Passmore, *Can. J. Chem*., 1979, **57**, 2714; j) M. Pasquali, C. Floriani and A. Gaetani-Manfredotti, *Inorg. Chem*., 1981, **20**, 3382; k) A. J. Lupinetti, G. Frenking and S. H. Strauss, *Angew. Chem., Int. Ed*., 1998, **37**, 2113; l) A. J. Lupinetti, S. H. Strauss and G. Frenking, *Prog. Inorg. Chem*., 2001, **49**, 1.

20. a) R. K. Szilagyi and G. Frenking, *Organometallics*, 1997, **16**, 4807; b) A. J. Lupinetti, V. Jonas, W. Thiel, S. H. Strauss and G. Frenking, *Chem. Eur. J*., 1999, **5**, 2573; c) A. Diefenbach, F. M. Bickelhaupt and G. Frenking, *J. Am. Chem. Soc*., 2000, **122**, 6449; d) A. J. Lupinetti, S. Fau, G. Frenking and S. H. Strauss, *J. Phys. Chem. A*, 1997, **101**, 9551; e) A. S. Goldman and K. Krogh-Jespersen, *J. Am. Chem. Soc*., 1996, **118**, 12159.

21. M. Chen, Q. Zhang, M. Zhou, D. M. Andrada and G. Frenking, *Angew. Chem., Int. Ed*., 2015, **54**, 124.

22. a) K. Morokuma, *Acc. Chem. Res*., 1977, **10**, 294; b) T. Ziegler and A. Rauk, *Theor. Chim. Acta*, 1977, **46**, 1; c) T. Ziegler, A. Rauk and E. J. Baerends, *Theor. Chim. Acta*, 1977, **43**, 261; d) M. von Hopffgarten and G. Frenking, *Wiley Interdiscip. Rev. Comput. Mol. Sci.*, 2012, **2**, 43.

23. a) M. P. Mitoraj, A. Michalak and T. Ziegler, *J. Chem. Theory Comput*., 2009, **5**, 962; b) M. P. Mitoraj and A. Michalak, *Organometallics*, 2007, **26**, 6576; c) M. P. Mitoraj and A. Michalak, *J. Mol. Model*., 2008, **14**, 681.

24. P. v. R. Schleyer, C. Maerker, A. Dransfeld, H. Jiao and N. J. R. v. E. Hommes, *J. Am. Chem. Soc*., 1996, **118**, 6317.

25. C. Corminboeuf, T. Heine, G. Seifert, P. v. R. Schleyer and J. Weber, *Phys. Chem. Chem.Phys.*, 2004, **6**, 273.

26. S. Noorizadeh and M. Dardab, *Chem. Phys. Lett*., 2010, **493**, 376.

27. J. J. Torres-Vega, A. Vásquez-Espinal, J. Caballero, M. L. Valenzuela, L. Alvarez-Thon, E. Osorio and W. Tiznado, *Inorg. Chem.*, 2014, **53**, 3579.

28. Y. Zhao and D. G. Truhlar, *Theor. Chem. Acc.*, 2008, **120**, 215.

29. F. Weigend and R. Ahlrichs, *Phys. Chem. Chem. Phys.*, 2005, **7**, 3297.

30. D. Andrae, U. Haeussermann, M. Dolg, H. Stoll and H. Preuss, *Theor. Chim. Acta*, 1990, **77**, 123.

31. S. F. Boys and F. Bernardi, *Mol. Phys.*, 1970, **19**, 553.

32. Gaussian 09, Revision C.01, M. J. Frisch, et al. Gaussian, Inc., Wallingford CT, 2009.

33. S. Grimme, J. Antony, S. Ehrlich and H, Krieg, *J. Chem. Phys.*, 2010, **132**, 154104.

34. a) ADF2013.01, E. J. Baerends, T. Ziegler, J. Autschbach, D. Bashford, A. Bérces, F. M. Bickelhaupt, C. Bo, P. M. Boerrigter, L. Cavallo, D. P. Chong, L. Deng, R. M. Dickson, D. E. Ellis, M. v. Faassen, L. Fan, T. H. Fischer, C. F. Guerra, A. Ghysels, A. Giammona, S. J. A. v. Gisbergen, A. W. Götz, J. A. Groeneveld, O. V. Gritsenko, M. Gr ning, S. Gusarov, F. E. Harris, P. v. d. Hoek, C. R. Jacob, H. Jacobsen, L. Jensen, J. W. Kaminski, G. v. Kessel, F. Kootstra, A. Kovalenko, M. V. Krykunov, E. v. Lenthe, D. A. McCormack, A. Michalak, M. Mitoraj, J. Neugebauer, V. P. Nicu, L. Noodleman, V. P. Osinga, S. Patchkovskii, P. H. T. Philipsen, D. Post, C. C. Pye, W. Ravenek, J. I. Rodríguez, P. Ros, P. R. T. Schipper, G. Schreckenbach, J. S. Seldenthuis, M. Seth, J. G. Snijders, M. Solà, M. Swart, D. Swerhone, G. t. Velde, P. Vernooijs, L. Versluis, L. Visscher, O. Visser, F. Wang, T. A. Wesolowski, E. M. v. Wezenbeek, G. Wiesenekker, S. K. Wolff, T. K. Woo, A. L. Yakovlev, SCM, Theoretical Chemistry, Vrije Universiteit, Amsterdam, The Netherlands, 2013; b) G. te Velde, F. M. Bickelhaupt, E. J. Baerends, C. F. Guerra, S. J. A. Van Gisbergen, J. G. Snijders and T. Ziegler, *J. Comput. Chem.*, 2001, **22**, 931.

35. a) E. van Lenthe, A. Ehlers and E. J. Baerends, *J. Chem. Phys.*, 1999, **110**, 8943; b) E. van Lenthe, E. J. Baerends and J. G. Snijders, *J. Chem. Phys.*, 1993, **99**, 4597; c) E. van Lenthe, E. J. Baerends and J. G. Snijders, *J. Chem. Phys.*, 1994, **101**, 9783; d) E. van Lenthe, J. G. Snijders and E. J. Baerends, *J. Chem. Phys.*, 1996, **105**, 6505; e) E. van Lenthe, R. v. Leeuwen, E. J. Baerends and J. G. Snijders, *Int. J. Quantum Chem.*, 1996, **57**, 281.

36. T. Lu and F. W. Chen, *J. Comput. Chem.*, 2012, **33**, 580.

37. a) J. Cioslowski and S. T. Mixon, *Can. J. Chem.* 1992, **70**, 443; b) J. Cioslowski and S. T. Mixon, *J. Am. Chem. Soc.* 1992, **114**, 4382; c) A. Haaland, D. J. Shorokhov and N. V. Tverdova, *Chem. Eur. J.* 2004, **10**, 4416; d) A. Krapp and G. Frenking, *Chem. Eur. J.*, 2007, **13**, 8256; e) J. Poater, R. Visser, M. Solà and F. M. Bickelhaupt, *J. Org. Chem.* 2007, **72**, 1134; f) E. Cerpa, A. Krapp, A. Vela and G. Merino, *Chem. Eur. J.* 2008, **14**, 10232; g) E. Cerpa, A. Krapp, R. Flores-Moreno, K. J. Donald and G. Merino, *Chem. Eur. J.* 2009, **15**, 1985; e) P. Macchi, D. M. Proserpio and A. J. Sironi, *J. Am. Chem. Soc.* 1998, **120**, 13429; f) P. Macchi, L. Garlaschelli, S. Martinengo and A. J. Sironi, *J. Am. Chem. Soc.* 1999, **121**, 10428; g) I. V. Novozhilova, A. V. Volkov and P. J. Coppens, *J. Am. Chem. Soc.* 2003, **125**, 1079; h) S. Pan, A. Gupta, S. Mandal, D. Moreno, G. Merino and P. K. Chattaraj, *Phys. Chem. Chem. Phys.* 2015, **17**, 972; i) S. Pan, D. Moreno, S. Ghosh, P. K. Chattaraj and G. Merino, *J. Comput. Chem.*, 2015, DOI: 10.1002/jcc.23986.

38. D. Cremer and E. Kraka, *Angew. Chem. Int. Ed.*, 1984, **23**, 627.

39. a) K. Wolinski, J. F. Hilton and P. Pulay, *J. Am. Chem. Soc.*, 1990, **112**, 8251; b) J. R. Cheeseman, G. W. Trucks, T. A. Keith and M. J. Frisch, *J. Chem. Phys.*, 1996, **104**, 5497.

40. M. Giambiagi, M. S. de Giambiagi and K. C. Mundim, *Struct. Chem.*, 1990, **1**, 423.

41. a) R. Ponec and I. Mayer, *J. Phys. Chem. A*, 1997, **101**, 1738; b) M. Giambiagi, M. S. d. Giambiagi, C. D. d. S. Silva and A. P. d. Figueiredo, *Phys. Chem. Chem. Phys.*, 2000, **2**, 3381.

42. T. A. Keith, AIMAll (Version 15.05.18), TK Gristmill Software, Overland Park KS, USA, 2015.

43. L. Yong, S. D. Wu and X. X. Chi, *Int. J. Quantum Chem.*, 2007, **107**, 722.

44. a) J. O. Hirschfelder, *J. Chem. Phys.*, 1938, **6**, 795; b) A. N. Alexandrova and A. I. Boldyrev, *J. Phys. Chem. A*, 2003, **107**, 554.

45. B. Cordero, V. Gómez, A. E. Platero-Prats, M. Revés, J. Echeverría, E. Cremades, F. Barragán and S. Alvarez, *Dalton Trans.*, 2008, **21**, 2832.

46. a) P. Schwerdtfeger, *Heteroat. Chem.*, 2002, **13**, 578; b) P . Schwerdtfeger, *Angew. Chem. Int. Ed.*, 2003, **42**, 1892; c) P. Pyykkö, Relativistic Theory of Atoms and Molecules, Vol. III, Springer, Berlin, 2000, pp. 108 – 111; c) H. Schwarz, *Angew. Chem. Int. Ed.*, 2003, **42**, 4442.

47. K. B. Wiberg, *Tetrahedron*, 1968, **24**, 1083.

48. R. W. A. Havenith, F. De Proft, P. W. Fowler and P. Geerlings, *Chem. Phys. Lett.*, 2005, **407**, 391.

49. a) L. Khriachtchev, M. Pettersson, J. Lundell, H. Tanskanen, T. Kiviniemi, N. Runeberg and M. Räsänen, *J. Am. Chem. Soc.*, 2003, **125**, 1454; b) L. Khriachtchev, H. Tanskanen, A. Cohen, R. B. Gerber, J. Lundell, M. Pettersson, H. Kiljunen and M. Räsänen, *J. Am. Chem. Soc.*, 2003, **125**, 6876; c) H. Tanskanen, L. Khriachtchev, J. Lundell, H. Kiljunen and M. Räsänen, *J. Am. Chem. Soc.*, 2003, **125**, 16361; d) V. I. Feldman, F. F. Sukhov, A. Yu. Orlov and I. V. Tyulpina, *J. Am. Chem. Soc.*, 2003, **125**, 4698; e) V. I. Feldman, A.V. Kobzarenko, I. A. Baranova, A. V. Danchenko, F. F. Sukhov, E. Tsivion and R. B. Gerber, *J. Chem. Phys.*, 2009, **131**, 151101; f) S. V. Ryazantsev, A. V. Kobzarenko and V. I. Feldman, *J. Chem. Phys.*, 2013, **139**, 124315; g) B. Liang, L. Andrews, J. Li and B. E. Bursten, *J. Am. Chem. Soc.*, 2002, **124**, 9016; h) X. Wang, L. Andrews, J. Li and B. E. Bursten, *Angew. Chem. Int. Ed.*, 2004, **43**, 2554; i) X. Wang, L. Andrews, K. Willmann, F. Brosi and S. Riedel, *Angew. Chem. Int. Ed.*, 2012, **51**, 10628; j) G. L. Smith, H. P. A. Mercier and G. J. Schrobilgen, *Inorg. Chem.*, 2011, **49**, 12359; k) D.S. Brock, H. P. A. Mercier and G. J. Schrobilgen, *J. Am. Chem. Soc.*, 2013, **135**, 5089; l) J. R. Debackere, H. P. A. Mercier and G. J. Schrobilgen, *J. Am. Chem. Soc.*, 2014, **136**, 3888; m) C. Ó. Jiménez-Halla, I. Fernández and G. Frenking, *Angew. Chem. Int. Ed.*, 2009, **48**, 366; n) L. A. Mück, A. Y. Timoshkin, M. v. Hopffgarten and G. Frenking, *J. Am. Chem. Soc.*, 2009, **131**, 3942; o) I. Fernández and G. Frenking, *Phys. Chem. Chem. Phys.*, 2012, **14**, 14869; p) Q. Zhang, M. Chen, M. Zhou, D. M. Andrada and G. Frenking, *J. Phys. Chem. A*, 2015, **119**, 2543; q) S. Pan, M. Contreras, J. Romero, A. Reyes, P. K. Chattaraj and G. Merino, *Chem. Eur. J.*, 2013, **19**, 2322; r) S. Pan, S. Jalife, R. M. Kumar, V. Subramanian, G. Merino and P. K. Chattaraj, *ChemPhysChem*, 2013, **14**, 2511; s) S. Pan, D. Moreno, J. L. Cabellos, J. Romero, A. Reyes, G. Merino and P. K. Chattaraj, *J. Phys. Chem. A*, 2014, **118**, 487; t) M. Khatua, S. Pan and P. K. Chattaraj, *J. Chem. Phys.*, 2014, **140**, 164306; u) S. Pan, D. Moreno, J. L. Cabellos, G. Merino and P. K. Chattaraj, *ChemPhysChem*, 2014, **15**, 2618; v) S. Pan, D. Moreno, G. Merino and P. K. Chattaraj, *ChemPhysChem*, 2014, **15**, 3554; w) L. Khriachtchev, M. Räsänen and R. B. Gerber, *Acc. Chem. Res.*, 2009, **42**, 183; x) W. Grochala, *Phys. Chem. Chem. Phys.*, 2012, **14**, 14860; y) L. Operti, R. Rabezzana, F. Turco, S. Borocci, M. Giordani and F. Grandinetti, *Chem. Eur. J.*, 2011, **17**, 10682; z) S. Borocci , M. Giordani and F. Grandinetti, *J. Phys. Chem. A*, 2015, **119**, 2383.

50. a) C. J. Evans, A. Lesarri and M. C. L. Gerry, *J. Am. Chem. Soc*., 2000, **122**, 6100; b) C. J. Evans and M. C. L. Gerry, *J. Chem. Phys*., 2000, **112**, 1321; c) C. J. Evans and M. C. L. Gerry, *J. Chem. Phys*., 2000, **112**, 9363; d) C. J. Evans, D. S. Rubinoff and M. C. L. Gerry, *Phys. Chem. Chem. Phys*., 2000, **2**, 3943; e) L. M. Reynard, C. J. Evans and M. C. L. Gerry*, J. Mol. Spectrosc*., 2001, **206**, 33; e) J. M. Michaud, S. A. Cooke and M. C. L. Gerry, *Inorg. Chem*., 2004, **43**, 3871; f) J. M. Thomas, N. R. Walker, S. A. Cooke and M. C. L. Gerry, *J. Am. Chem. Soc*., 2004, **126**, 1235; g) C. J. Evans , T. G. Wright and A. M. Gardner, *J. Phys. Chem. A*, 2010, **114**, 4446; h) S. M. Beyhan, A. W. Götz, C. R. Jacob and L. Visscher, *J. Chem. Phys*., 2010, **132**, 044114; i) S. Pan, A. Gupta, R. Saha, G. Merino and P. K. Chattaraj *J. Comp. Chem*., 2015, **36**, 2168.

51. L. Belpassi, I. Infante, F. Tarantelli and L. Visscher, *J. Am. Chem. Soc*., 2008, **130**, 1048.

52. a) T. A. Albright, J. K. Burdett and M. H. Whangbo, Orbital Interactions in Chemistry, *Wiley*, New York, 1985, p. 82; b) U. Radius, F. M. Bickelhaupt, A.W. Ehlers, N. Goldberg and R. Hoffmann, *Inorg. Chem*., 1998, **37**, 1080.

53. a) G. Herzberg, Spectra of Diatomic Molecules, 2nd. Ed.; Van Nostrand: New York, 1950; b) E. Hirota and J. Endo, *J. Mol. Spectrosc*., 1988, **127**, 524.

54. G. Frenking, C. Loschen, A. Krapp, S. Fau and S. H. Strauss, *J. Comput. Chem*., 2007, **28**, 117.

Figures
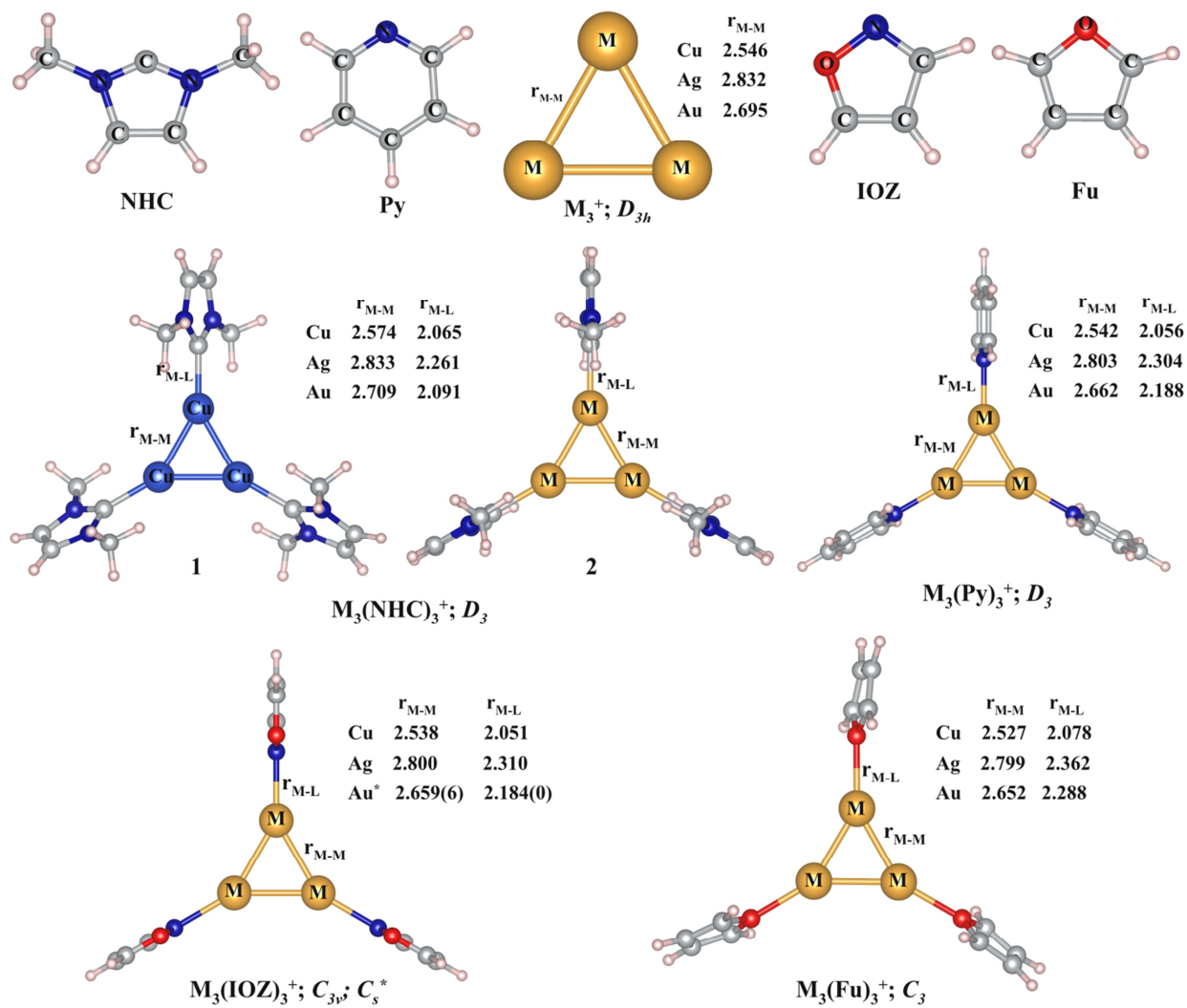
Fig. 1 Pictorial depiction of M_3^+, L and $M_3L_3^+$ complexes. M-M and M-L bond distances in Å are also provided at the M06-2X/def2-TZVP level.
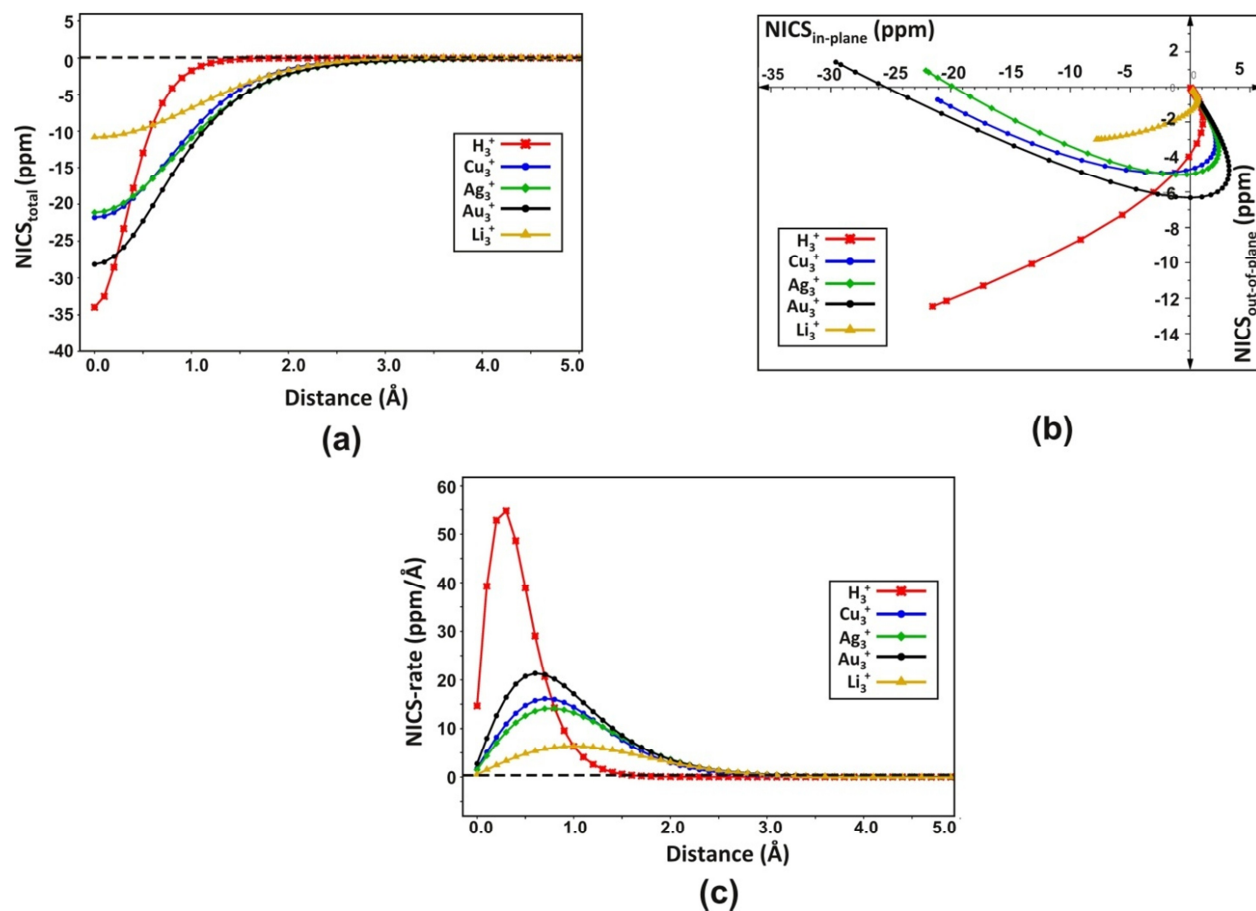
Fig. 2 Different NICS plots for the H_3^+, Li_3^+, Cu_3^+, Ag_3^+ and Au_3^+ clusters. (a) NICS$_{total}$-scan plot (b) FiPC-NICS plots (c) NICS-rate plots at the M06-2X/def2-TZVP level.
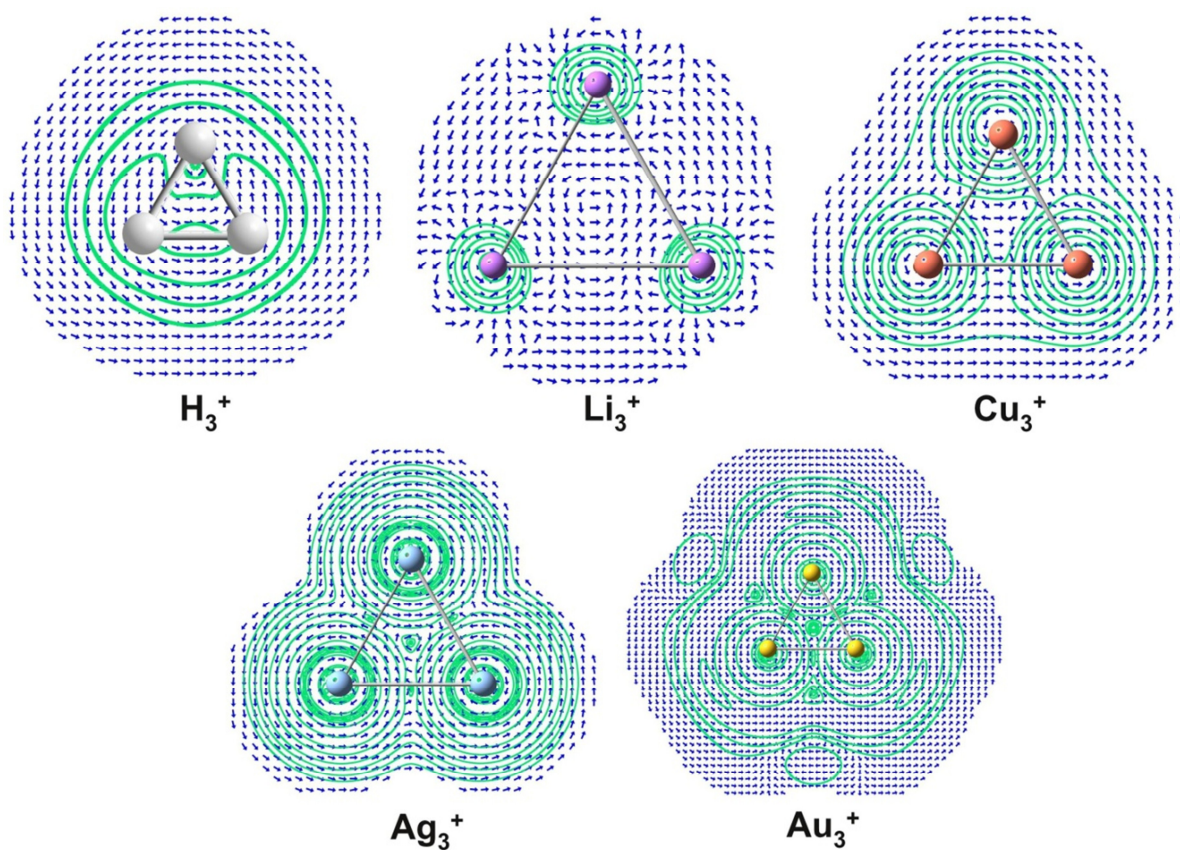
Fig. 3 Ring current density plots for H_3^+, Li_3^+, Cu_3^+, Ag_3^+ and Au_3^+ clusters at the M06-2X/def2-TZVP level.

Fig.4 The plots of deformation density ($\Delta\rho(r)$) for $M_3(NHC)_3^+$ and $M_3(Py)_3^+$ complexes at the PBE-D3/TZ2P//M06-2X/def2-TZVP level. (An isovalue of 0.001 is used.)
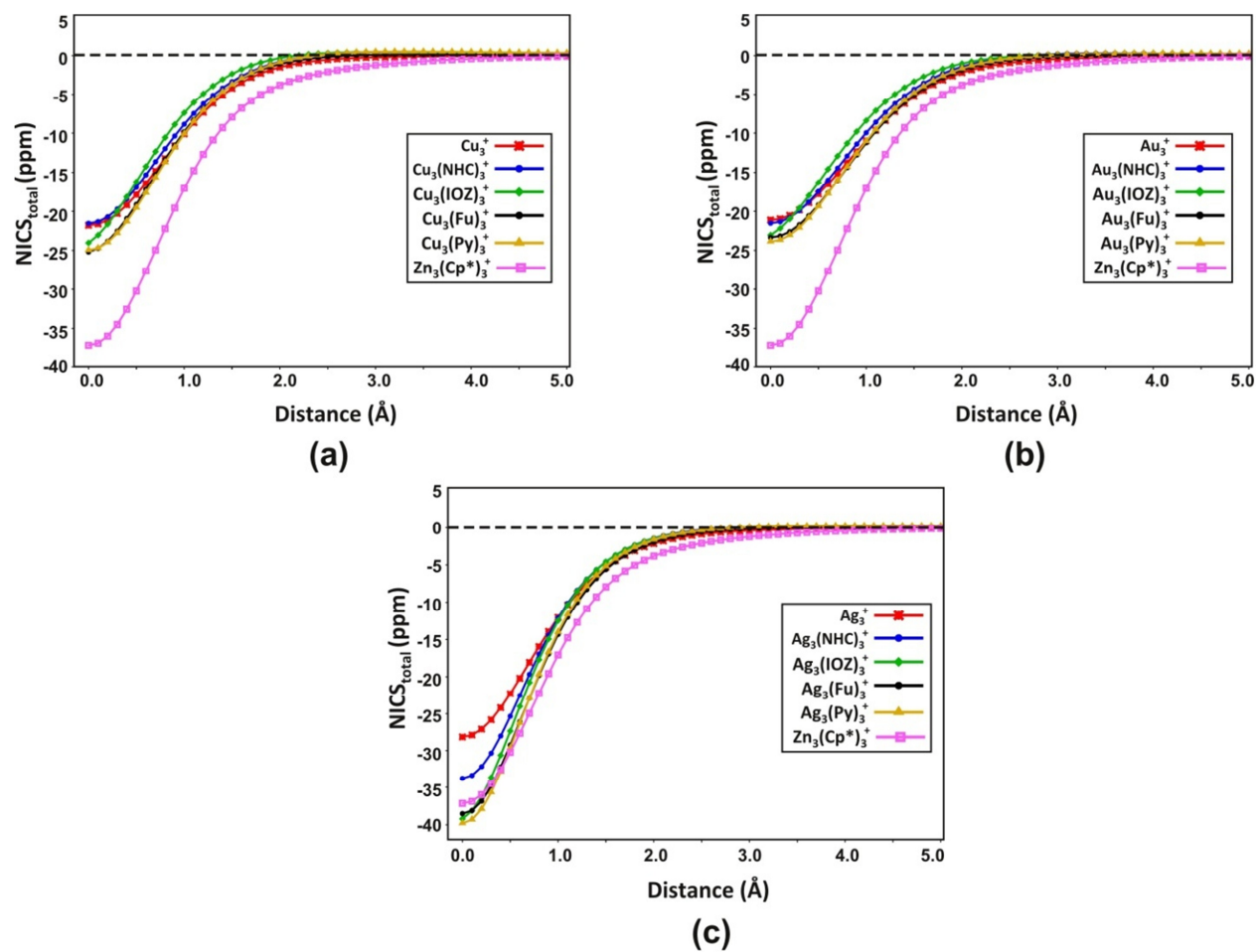
Fig. 5 NICS$_{total}$-scan plots for the M$_3$L$_3^+$ complexes at the M06-2X/def2-TZVP level.
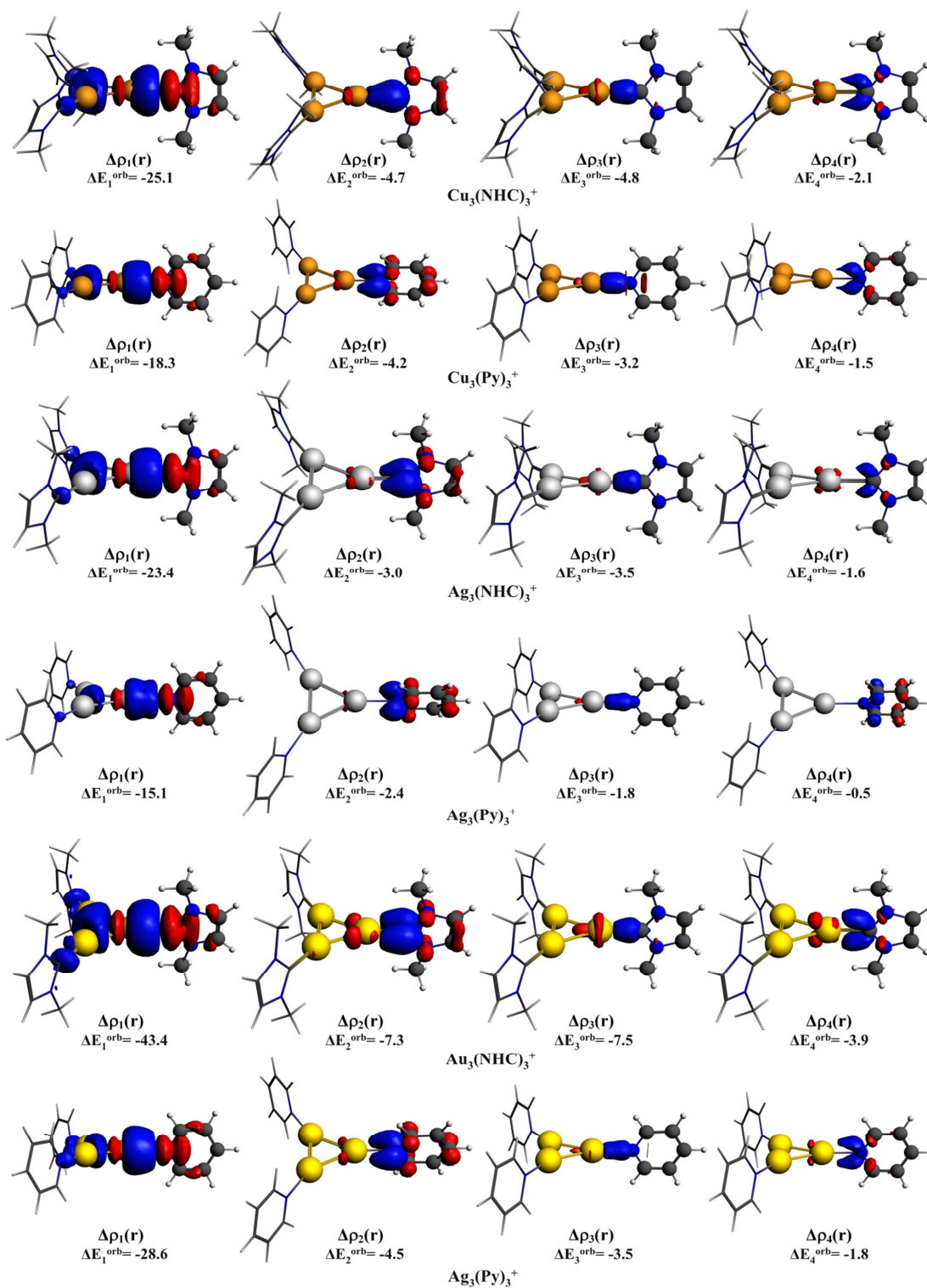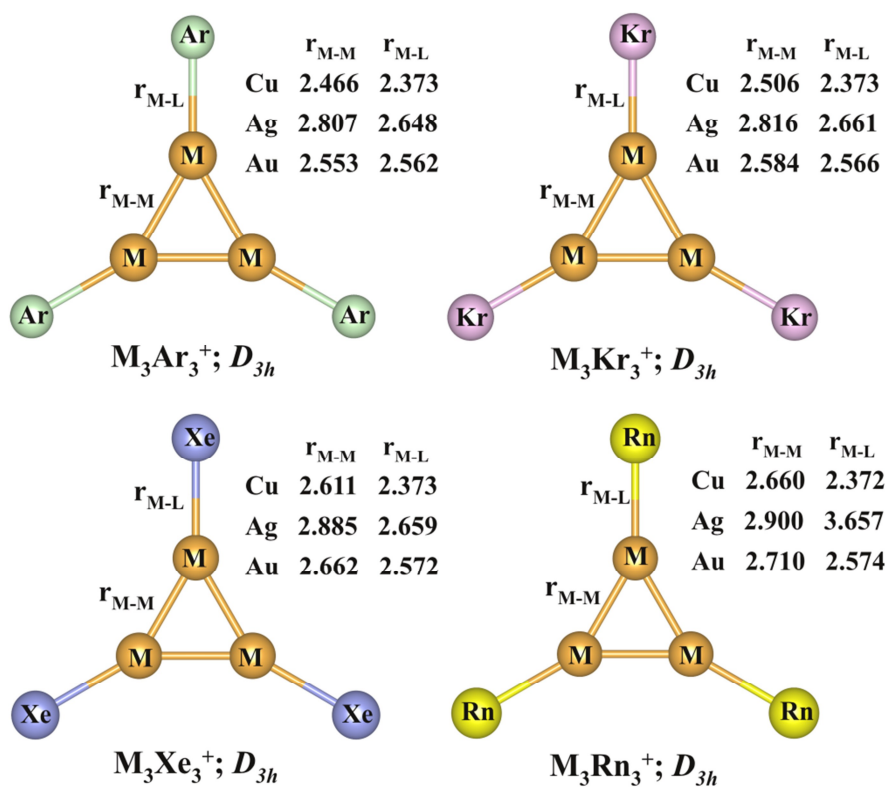
Fig. 6 Pictorial depiction of $M_3Ng_3^+$ complexes. M-M and M-Ng bond distances in Å are also provided at the MP2/def2-TZVP level.

$\Delta E^{\sigma}= -7.7$
$Cu_3Ar_3^+$

$\Delta E^{\sigma}= -10.5$
$Cu_3Kr_3^+$

$\Delta E^{\sigma}= -15.1$
$Cu_3Xe_3^+$

$\Delta E^{\sigma}= -16.9$
$Cu_3Rn_3^+$

$\Delta E^{\sigma}= -4.6$
$Ag_3Ar_3^+$

$\Delta E^{\sigma}= -7.2$
$Ag_3Kr_3^+$

$\Delta E^{\sigma}= -10.5$
$Ag_3Xe_3^+$

$\Delta E^{\sigma}= -12.5$
$Ag_3Rn_3^+$

$\Delta E^{\sigma}= -11.1$
$Au_3Ar_3^+$

$\Delta E^{\sigma}= -15.6$
$Au_3Kr_3^+$

$\Delta E^{\sigma}= -21.3$
$Au_3Xe_3^+$

$\Delta E^{\sigma}= -23.7$
$Au_3Rn_3^+$

Fig. 7 The plots of deformation density ($\Delta\rho(r)$) for $M_3Ng_3^+$ complexes at the PBE-D3/TZ2P//MP2/def2-TZVP level. (An isovalue of 0.001 is used.)

Fig. 8 Pictorial depiction of $M_3(CO)_3^+$ and $M_3(OC)_3^+$ complexes. M-M, M-C and C-O bond distances in Å are also provided at the M06-2X/def2-TZVP level.
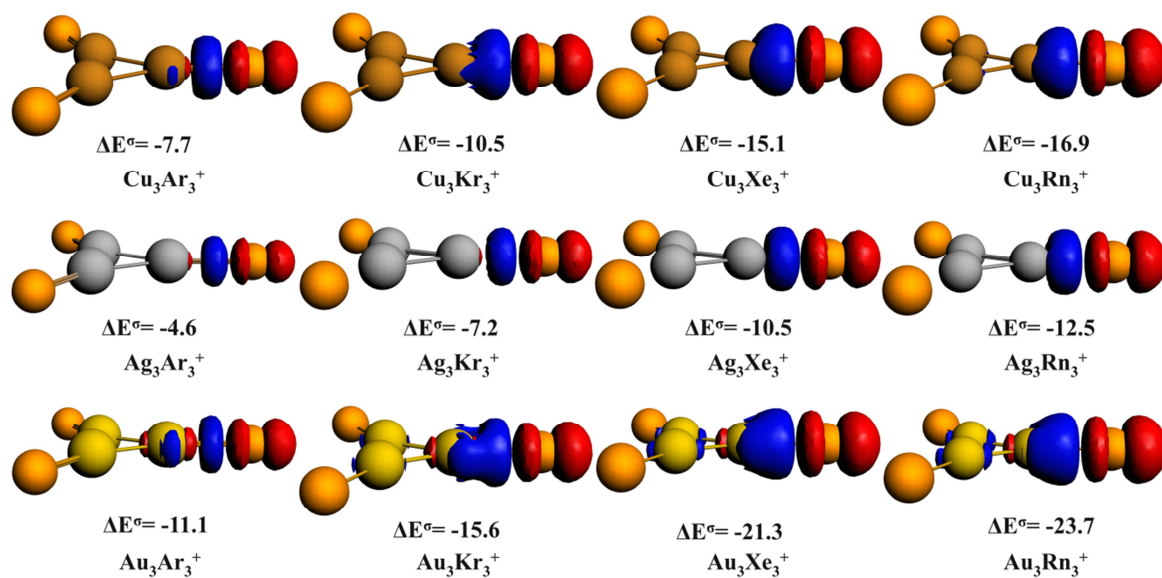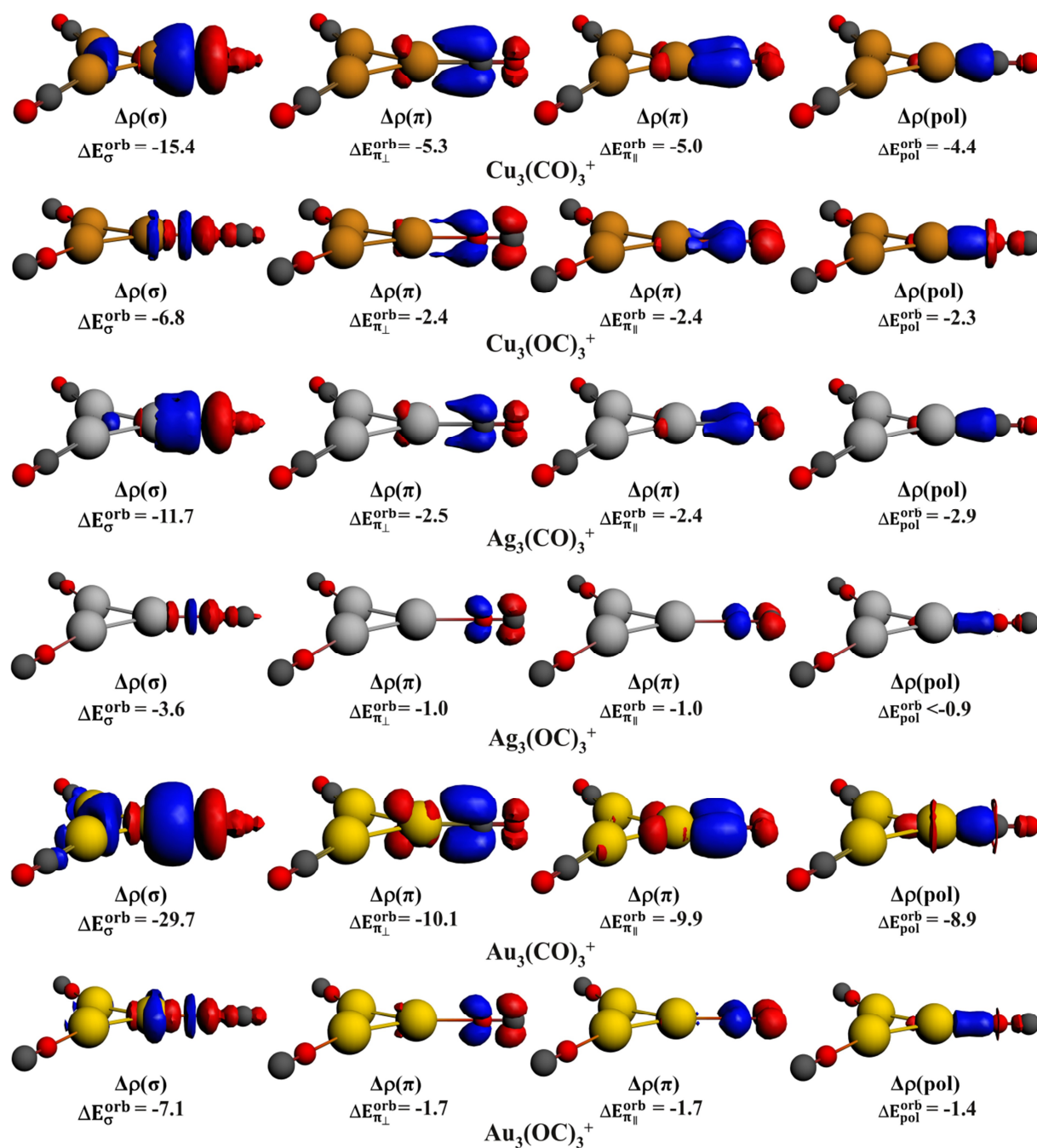
Fig. 9 The plots of deformation density ($\Delta\rho(r)$) for $M_3(CO)_3^+$ and $M_3(OC)_3^+$ complexes at the PBE-D3/TZ2P//M06-2X/def2-TZVP level. (An isovalue of 0.001 is used.)

Tables

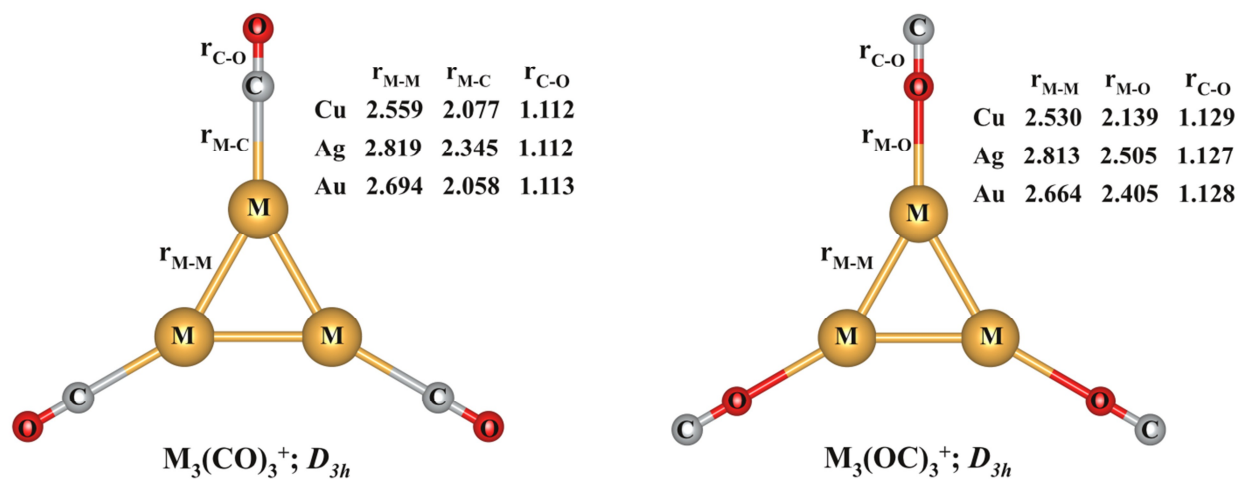**Table 1.** Both ZPE and BSSE corrected dissociation energy (D_0^{BSSE}, kcal/mol), dissociation enthalpy (ΔH, kcal/mol), and free energy change (ΔG, kcal/mol) per L for the dissociation process at 298 K: $M_3L_3^+ \rightarrow 3\,L + M_3^+$, NPA charge at M center and L (q, au), Wiberg bond indices of M-L and M-M bonds (WBI), HOMO-LUMO energy gap (Gap, eV), electron affinity (EA, eV), M-M (r_{M-M}, Å) and M-L bond distances (r_{M-L}, Å) at the M06-2X/def2-TZVP level.

Clusters	PG	D_0^{BSSE}	ΔH	ΔG	q_L	q_M	WBI_{M-L}	WBI_{M-M}	Gap	EA	r_{M-M}	r_{M-L}
Cu_3^+	D_{3h}					0.33		0.46	5.78	6.64	2.546	
$Cu_3(NHC)_3^+$	D_3	51.5	51.8	41.6	0.22	0.11	0.37	0.39	5.60	2.36	2.574	2.065
$Cu_3(Py)_3^+$	D_3	36.7	36.9	26.2	0.09	0.24	0.17	0.43	5.80	3.20	2.542	2.056
$Cu_3(IOZ)_3^+$	C_{3v}	33.1	33.2	23.7	0.10	0.24	0.19	0.43	6.07	3.08	2.538	2.051
$Cu_3(Fu)_3^+$	C_3	19.7	19.6	10.8	0.06	0.28	0.09	0.44	6.43	3.84	2.527	2.078
Ag_3^+	D_{3h}					0.33		0.46	5.33	6.43	2.832	
$Ag_3(NHC)_3^+$	D_3	43.6	43.5	33.6	0.23	0.11	0.35	0.43	5.41	2.56	2.833	2.261
$Ag_3(Py)_3^+$	D_3	28.4	28.1	18.5	0.09	0.25	0.13	0.44	5.76	3.27	2.803	2.304
$Ag_3(IOZ)_3^+$	C_{3v}	25.1	24.8	15.8	0.09	0.24	0.15	0.44	5.85	3.30	2.800	2.310
$Ag_3(Fu)_3^+$	C_3	13.5	13.1	4.7	0.05	0.29	0.07	0.45	5.86	4.38	2.799	2.362
Au_3^+	D_{3h}					0.33		0.49	6.22	7.52	2.695	
$Au_3(NHC)_3^+$	D_3	64.1	63.9	52.3	0.31	0.02	0.51	0.44	6.88	2.40	2.709	2.091
$Au_3(Py)_3^+$	D_3	39.2	39.5	28.7	0.14	0.19	0.22	0.46	7.39	3.29	2.662	2.188
$Au_3(IOZ)_3^+$	C_s	34.3	34.7	24.4	0.14	0.20	0.24	0.46	7.72	3.24	2.659(6)	2.184(0)
$Au_3(Fu)_3^+$	C_3	18.1	18.2	9.4	0.07	0.26	0.11	0.48	6.57	4.44	2.652	2.288

Table 2. Electron density descriptors (au) at the bond critical points (BCP) of M-M and M-L bonds obtained from the wave functions generated at the M06-2X/def2-TZVP level.

Complexes	M-M			M-L		
	$\rho(r_c)$	$\nabla^2\rho(r_c)$	$H(r_c)$	$\rho(r_c)$	$\nabla^2\rho(r_c)$	$H(r_c)$
Cu_3^+	0.034	0.060	-0.005			
$Cu_3(NHC)_3^+$	0.038	0.024	-0.008	0.083	0.272	-0.026
$Cu_3(Py)_3^+$	0.038	0.039	-0.007	0.075	0.341	-0.018
$Cu_3(IOZ)_3^+$	0.039	0.040	-0.008	0.073	0.354	-0.016
$Cu_3(Fu)_3^+$	0.038	0.050	-0.007	0.059	0.337	-0.009
Ag_3^+	0.031	0.074	-0.004			
$Ag_3(NHC)_3^+$	0.035	0.058	-0.006	0.073	0.239	-0.014
$Ag_3(Py)_3^+$	0.036	0.069	-0.006	0.058	0.249	-0.007
$Ag_3(IOZ)_3^+$	0.036	0.070	-0.006	0.056	0.251	-0.004
$Ag_3(Fu)_3^+$	0.035	0.074	-0.006	0.043	0.214	-0.002
Au_3^+	0.056	0.140	-0.011			
$Au_3(NHC)_3^+$	0.060	0.100	-0.014	0.123	0.248	-0.053
$Au_3(Py)_3^+$	0.064	0.122	-0.016	0.089	0.319	-0.022
$Au_3(IOZ)_3^+$	0.065	0.124	-0.016	0.087	0.339	-0.020
$Au_3(Fu)_3^+$	0.065	0.135	-0.015	0.059	0.280	-0.007

Table 3. EDA-NOCV results of $M_3L_3^+$ complexes considering L as one fragment and $M_3L_2^+$ as another fragment at the PBE-D3/TZ2P//M06-2X/def2-TZVP level. All energy terms are in kcal/mol.

Clusters	ΔE^{Pauli}	[a]ΔE^{elstat}	[a]ΔE^{orb}_{total}	[b]ΔE^{orb}_1	[b]ΔE^{orb}_2	[b]ΔE^{orb}_3	[b]ΔE^{orb}_4	ΔE^{orb}_{res}	[a]ΔE^{disp}	ΔE^{in}
$Cu_3(NHC)_3^+$	89.1	-101.4 (70.0)	-40.1 (27.7)	-25.1(62.6)	-4.7(11.7)	-4.8(12.0)	-2.1(5.2)	-3.4	-3.4 (2.3)	-55.8
$Cu_3(Py)_3^+$	60.1	-67.2 (67.8)	-29.9 (30.2)	-18.3(61.2)	-4.2(14.0)	-3.2(10.7)	-1.5(5.0)	-2.7	-2.0 (2.0)	-39.0
$Cu_3(IOZ)_3^+$	52.9	-58.1 (66.1)	-28.4 (32.3)	-16.2(57.0)	-4.5(15.8)	-2.7(9.5)	-3.0(10.6)	-2.0	-1.4 (1.5)	-35.0
$Cu_3(Fu)_3^+$	35.3	-34.1 (60.9)	-20.1 (36.0)	-10.9(54.2)	-3.0(14.9)	-2.5(12.4)	-1.6(8.0)	-2.1	-1.8 (3.1)	-20.6
$Ag_3(NHC)_3^+$	87.3	-94.6 (71.6)	-34.7 (26.3)	-23.4(67.4)	-3.0(8.6)	-3.5(10.1)	-1.6(4.6)	-3.2	-2.8 (2.1)	-44.8
$Ag_3(Py)_3^+$	48.2	-52.8 (68.8)	-22.3 (29.1)	-15.1(67.7)	-2.4(10.8)	-1.8(8.1)	-0.5(2.2)	-2.5	-1.7 (2.2)	-28.5
$Ag_3(IOZ)_3^+$	40.5	-44.1 (67.1)	-20.1 (30.7)	-12.8(63.7)	-2.5(12.4)	-1.9(9.5)	-1.2(6.0)	-1.7	-1.5 (2.3)	-25.2
$Ag_3(Fu)_3^+$	23.6	-22.9 (61.4)	-12.8 (34.4)	-7.6(59.4)	-1.7(13.3)	-1.7(13.3)	-0.8(6.3)	-1.0	-1.6 (4.2)	-13.7
$Au_3(NHC)_3^+$	185.2	-180.5 (71.9)	-66.9 (26.6)	-43.3(64.7)	-7.3(10.9)	-7.5(11.2)	-3.9(5.8)	-4.5	-3.6 (1.4)	-65.7
$Au_3(Py)_3^+$	88.3	-86.7 (66.5)	-41.4 (31.8)	-28.6(69.1)	-4.5(10.9)	-3.5(8.5)	-1.8(4.3)	-3.0	-2.1 (1.6)	-41.9
$Au_3(IOZ)_3^+$	77.8	-74.6 (64.6)	-39.0 (33.8)	-25.2(64.6)	-4.8(12.3)	-3.2(8.2)	-3.4(8.7)	-2.4	-1.9 (1.6)	-37.7
$Au_3(Fu)_3^+$	38.1	-34.0 (58.6)	-22.1 (38.0)	-14.1(63.8)	-2.6(11.8)	-1.9(8.6)	-1.4(6.3)	-2.1	-2.0 (3.4)	-19.9

([a]The values within the parentheses are in percentage and show the contribution towards the total attractive interaction $\Delta E^{elstat} + \Delta E^{orb}_{total} + \Delta E^{disp}$; [b]the values within parentheses are the percentage contribution towards ΔE^{orb}_{total})

Table 4. Both ZPE and BSSE corrected dissociation energy (D_0^{BSSE}, kcal/mol), dissociation enthalpy (ΔH, kcal/mol), and free energy change (ΔG, kcal/mol) per Ng for the dissociation process at 298 K: $M_3Ng_3^+ \rightarrow 3\ Ng + M_3^+$, NPA charge at M and Ng centers (q, au), Wiberg bond indices of M-Ng bonds (WBI_{M-Ng}), HOMO-LUMO energy gap (Gap, eV), electron affinity (EA, eV), M-M (r_{M-M}, Å) and M-Ng bond distances (r_{M-Ng}, Å) at the MP2/def2-TZVP level.

Clusters	D_0^{BSSE}	ΔH	ΔG	q_{Ng}	q_M	WBI_{M-Ng}	Gap	EA	r_{M-Ng}	r_{M-M}
Cu_3^+					0.33		8.76	4.04		2.39
$Cu_3Ar_3^+$	3.9	5.1	-0.9	0.06	0.27	0.11	9.36	2.75	2.47	2.37
$Cu_3Kr_3^+$	6.4	8.0	1.8	0.09	0.24	0.17	9.38	2.44	2.51	2.37
$Cu_3Xe_3^+$	9.6	11.5	5.2	0.13	0.20	0.24	9.30	2.18	2.61	2.37
$Cu_3Rn_3^+$	11.2	14.0	7.6	0.15	0.19	0.26	9.15	2.16	2.66	2.37
Ag_3^+					0.33		8.21	4.03		2.68
$Ag_3Ar_3^+$	2.2	3.1	-2.2	0.04	0.29	0.08	8.62	3.21	2.81	2.65
$Ag_3Kr_3^+$	3.9	5.3	-0.4	0.07	0.26	0.13	8.69	2.90	2.82	2.66
$Ag_3Xe_3^+$	6.5	8.2	2.3	0.11	0.22	0.20	8.68	2.62	2.89	2.66
$Ag_3Rn_3^+$	8.1	10.6	4.6	0.13	0.20	0.23	8.61	2.54	2.90	2.66
Au_3^+					0.33		9.12	4.91		2.57
$Au_3Ar_3^+$	5.4	7.7	1.2	0.08	0.26	0.14	10.54	3.30	2.55	2.56
$Au_3Kr_3^+$	9.8	13.0	6.2	0.12	0.21	0.21	10.64	2.93	2.58	2.57
$Au_3Xe_3^+$	15.9	19.5	12.6	0.19	0.14	0.32	10.54	2.61	2.66	2.57
$Au_3Rn_3^+$	19.0	23.4	16.5	0.21	0.12	0.35	10.33	2.56	2.71	2.57

Table 5. EDA results of $M_3Ng_3^+$ complexes considering Ng as one fragment and $M_3Ng_2^+$ as another fragment at the PBE-D3/TZ2P//MP2/def2-TZVP level. All energy terms are in kcal/mol.

Clusters	ΔE^{Pauli}	ΔE^{elstat}	ΔE^{orb}	ΔE^{disp}	ΔE^{int}
$Cu_3Ar_3^+$	17.0	-11.2 (46.6)	-12.5 (51.7)	-0.4 (1.7)	-7.2
$Cu_3Kr_3^+$	25.1	-17.2 (48.8)	-17.4 (49.6)	-0.6 (1.6)	-10.1
$Cu_3Xe_3^+$	32.1	-22.8 (48.4)	-23.5 (50.0)	-0.8 (1.6)	-14.9
$Cu_3Rn_3^+$	35.7	-25.6 (49.6)	-25.1 (48.6)	-0.9 (1.8)	-16.0
$Ag_3Ar_3^+$	8.0	-5.3 (42.6)	-6.6 (53.0)	-0.6 (4.4)	-4.5
$Ag_3Kr_3^+$	15.1	-10.4 (46.3)	-11.4 (50.7)	-0.7 (2.9)	-7.3
$Ag_3Xe_3^+$	23.0	-16.4 (49.7)	-15.9 (47.9)	-0.8 (2.4)	-10.1
$Ag_3Rn_3^+$	28.9	-21.1 (52.2)	-18.3 (45.3)	-1.0 (2.5)	-11.4
$Au_3Ar_3^+$	28.2	-17.1 (48.6)	-17.6 (49.9)	-0.5 (1.5)	-7.0
$Au_3Kr_3^+$	42.3	-27.4 (50.9)	-25.8 (47.8)	-0.7 (1.4)	-11.6
$Au_3Xe_3^+$	60.0	-41.2 (53.9)	-34.2 (44.8)	-1.0 (1.3)	-16.4
$Au_3Rn_3^+$	66.4	-46.7 (55.5)	-36.3 (43.1)	-1.2 (1.5)	17.9

(The values within the parentheses are in percentage and show the contribution towards the total attractive interaction $\Delta E^{elstat} + \Delta E^{orb} + \Delta E^{disp}$)

Table 6. Electron density descriptors (au) at the bond critical points (BCP) of M-M and M-Ng bonds obtained from the wave functions generated at the MP2/def2-TZVP level. The differences between r_{M-Ng} and typical M-Ng covalent bond distances ($r_{M-Ng}-r_{cov}$) are also provided.

Complexes	M-M			M-Ng			$r_{M-Ng}-r_{cov}$
	$\rho(r_c)$	$\nabla^2\rho(r_c)$	$H(r_c)$	$\rho(r_c)$	$\nabla^2\rho(r_c)$	$H(r_c)$	
Cu_3^+	0.049	0.108	-0.009				
$Cu_3Ar_3^+$	0.052	0.106	-0.011	0.036	0.177	-0.001	0.39
$Cu_3Kr_3^+$	0.052	0.104	-0.011	0.043	0.175	-0.005	0.22
$Cu_3Xe_3^+$	0.053	0.102	-0.011	0.046	0.147	-0.007	0.18
$Cu_3Rn_3^+$	0.053	0.102	-0.011	0.046	0.134	-0.008	0.12
Ag_3^+	0.043	0.108	-0.009				
$Ag_3Ar_3^+$	0.044	0.110	-0.009	0.022	0.095	0.000	0.57
$Ag_3Kr_3^+$	0.045	0.110	-0.010	0.030	0.109	-0.002	0.37
$Ag_3Xe_3^+$	0.045	0.109	-0.010	0.035	0.104	-0.004	0.30
$Ag_3Rn_3^+$	0.046	0.109	-0.010	0.038	0.102	-0.005	0.20
Au_3^+	0.073	0.182	-0.021				
$Au_3Ar_3^+$	0.076	0.175	-0.023	0.049	0.198	-0.006	0.35
$Au_3Kr_3^+$	0.076	0.169	-0.023	0.059	0.187	-0.011	0.17
$Au_3Xe_3^+$	0.075	0.165	-0.023	0.065	0.150	-0.016	0.11
$Au_3Rn_3^+$	0.075	0.164	-0.022	0.065	0.132	-0.017	0.05

Table 7. Both ZPE and BSSE corrected dissociation energy (D_0^{BSSE}, kcal/mol), dissociation enthalpy (ΔH, kcal/mol), and free energy change (ΔG, kcal/mol) per CO for the dissociation process at 298 K: $M_3(CO)_3^+/M_3(OC)_3^+ \rightarrow 3\ CO + M_3^+$, NPA charges at M, C, O and CO (q, au), charge separation in CO (Δq_{C-O}, au), Wiberg bond indices of M-C/O bonds (WBI), HOMO-LUMO energy gap (Gap, eV), M-M, M-C/O and C-O bond distances (r, Å) and vibrational frequency corresponding to the C-O symmetric (A_1') and asymmetric (E') stretching mode (ν_{CO}, cm^{-1}) at the M06-2Xdef2-TZVP level.

Clusters	D_0^{BSSE}	ΔH	ΔG	q_C	q_O	q_{CO}	q_M	Δq_{C-O}	WBI	Gap	$r_{M-C/O}$	r_{C-O}	r_{M-M}	ν_{CO}	
														E'	A_1'
CO				0.50	-0.50	0.00		1.00				1.120			
Cu$_3^+$							0.33			5.78			2.546		
Cu$_3$(CO)$_3^+$	18.6	19.1	10.3	0.52	-0.36	0.16	0.17	0.88	0.37	5.97	2.077	1.112	2.559	2348 (79)	2351 (82)
Cu$_3$(OC)$_3^+$	8.2	8.3	0.7	0.66	-0.61	0.04	0.29	1.27	0.08	6.39	2.139	1.129	2.530	2199 (-70)	2203 (-66)
Ag$_3^+$							0.33			5.33			2.832		
Ag$_3$(CO)$_3^+$	12.4	12.4	4.2	0.53	-0.38	0.15	0.18	0.91	0.31	5.76	2.345	1.112	2.819	2346 (77)	2347 (78)
Ag$_3$(OC)$_3^+$	4.7	4.6	-2.3	0.63	-0.59	0.04	0.29	1.22	0.06	5.72	2.505	1.127	2.813	2214 (-55)	2217 (-52)
Au$_3^+$							0.33			6.22			2.695		
Au$_3$(CO)$_3^+$	24.0	24.8	15.5	0.54	-0.33	0.20	0.13	0.87	0.55	7.64	2.058	1.113	2.694	2328 (59)	2339 (70)
Au$_3$(OC)$_3^+$	6.6	7.0	-0.9	0.65	-0.60	0.05	0.28	1.25	0.08	7.23	2.405	1.128	2.664	2202 (-67)	2206 (-63)

(The values in parentheses show the amount of red or blue shifting in frequency compared to that of free CO stretching frequency, 2269 cm^{-1})

Table 8. EDA-NOCV results of $M_3(CO)_3^+/M_3(OC)_3^+$ complexes considering CO as one fragment and $M_3(CO)_2^+/M_3(OC)_2^+$ as another fragment at the PBE-D3/TZ2P//M06-2X/def2-TZVP level. All energy terms are in kcal/mol.

| Clusters	ΔE^{Pauli}	[a]ΔE^{elstat}	[a]ΔE^{orb}_{total}	[a]ΔE^{disp}	ΔE^{int}	[b]ΔE^{orb}_{σ}	[b]$\Delta E^{orb}_{\pi_\perp}$	[b]$\Delta E^{orb}_{\pi_\parallel}$	[b]ΔE^{orb}_{pol}
Cu$_3$(CO)$_3^+$	47.3	-45.3(59.3)	-30.6(40.1)	-0.5(0.7)	-29.2	-15.4(50.4)	-5.3(17.2)	-5.0(16.3)	-4.4(14.4)
Cu$_3$(OC)$_3^+$	22.3	-16.5(52.8)	-14.3(45.5)	-0.5(1.7)	-9.1	-6.8(47.7)	-2.4 (16.8)	-2.4(16.5)	-2.3(15.8)
Ag$_3$(CO)$_3^+$	35.6	-33.0(61.3)	-20.1(37.5)	-0.6(1.2)	-18.2	-11.7(58.0)	-2.5 (12.6)	-2.4(12.2)	-2.9(14.2)
Ag$_3$(OC)$_3^+$	10.9	-8.4(53.7)	-6.5(42.0)	-0.7(4.3)	-4.6	-3.6(54.6)	-1.0 (14.9)	-1.0(14.9)	-a-
Au$_3$(CO)$_3^+$	119.5	-97.3(61.6)	-59.7(37.8)	-0.9(0.6)	-38.4	-29.7(49.8)	-10.1 (17.0)	-9.9 (16.6)	-8.9(14.9)
Au$_3$(OC)$_3^+$	19.3	-13.6 (51.0)	-12.3(46.1)	-0.8(2.9)	-7.4	-7.1(57.6)	-1.7(13.6)	-1.7(13.5)	-1.4(11.5)

([a]The values within the parentheses are in percentage and show the contribution towards the total attractive interaction $\Delta E^{elstat} + \Delta E^{orb}_{total} + \Delta E^{disp}$; [b] the values within parentheses are the percentage contribution towards ΔE^{orb}_{total}); -a- the corresponding value is below the cut-off value of ADF to be listed in the EDA-NOCV results.

Table 9. Electron density descriptors (au) at the bond critical points (BCP) of M-M and M-C/O bonds obtained from the wave functions generated at the M06-2X/def2-TZVP level.

Complexes	M-M			M-C/O		
	$\rho(r_c)$	$\nabla^2\rho(r_c)$	$H(r_c)$	$\rho(r_c)$	$\nabla^2\rho(r_c)$	$H(r_c)$
Cu_3^+	0.034	0.060	-0.006			
$Cu_3(CO)_3^+$	0.038	0.030	-0.008	0.073	0.290	-0.020
$Cu_3(OC)_3^+$	0.038	0.052	-0.007	0.046	0.288	-0.003
Ag_3^+	0.031	0.074	-0.005			
$Ag_3(CO)_3^+$	0.035	0.065	-0.006	0.055	0.211	-0.007
$Ag_3(OC)_3^+$	0.033	0.074	-0.005	0.028	0.143	0.001
Au_3^+	0.056	0.140	-0.010			
$Au_3(CO)_3^+$	0.062	0.138	-0.015	0.122	0.322	-0.054
$Au_3(OC)_3^+$	0.061	0.104	-0.014	0.041	0.211	-0.001

Graphical abstract
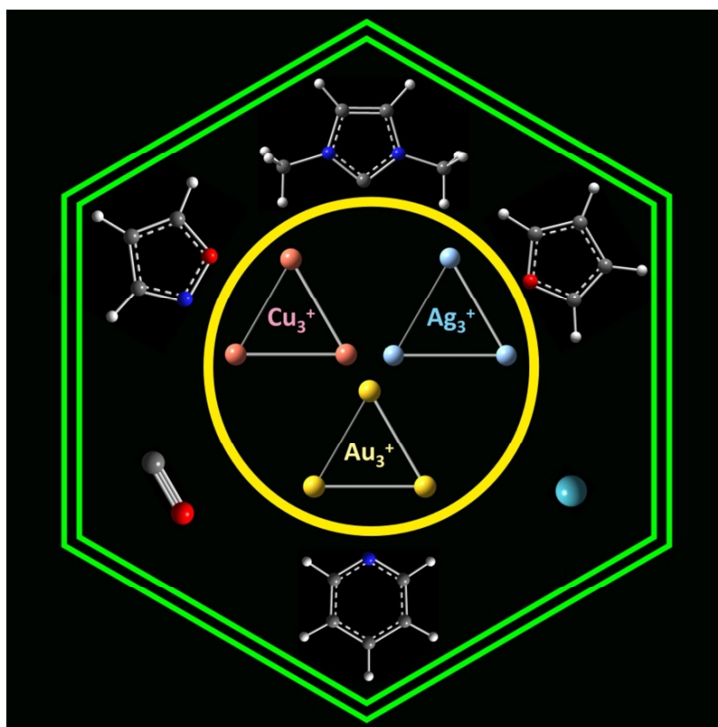
The structure, stability, bonding and σ-aromaticity in dimethyl imidazol-2-ylidene, pyridine, isoxazole, furan, noble gas and carbon monoxide bound M_3^+ (M = Cu, Ag, Au) complexes are analyzed.